Biomedicine & Pharmacotherapy 174 (2024) 116492

Contents lists available at ScienceDirect

Biomedicine & Pharmacotherapy

journal homepage: www.elsevier.com/locate/biopha

BET inhibitor nanotherapy halts kidney damage and reduces chronic kidney disease progression after ischemia-reperfusion injury

Maria Laura Saiz [a,b,1], Laura Lozano-Chamizo [c,d,e,1], Aida Bernardo Florez [a,b], Marzia Marciello [c,d], Paula Diaz-Bulnes [a,b], Viviana Corte-Iglesias [a,b,f], Cristian Ruiz Bernet [a,b], Raul R. Rodrigues-Diez [a,b], Cristina Martin-Martin [a,b], Mar Rodriguez-Santamaria [g], Ivan Fernandez-Vega [h,i], Ramon M. Rodriguez [j,k], Carmen Diaz-Corte [a,l], Beatriz Suarez-Alvarez [a,b,*], Marco Filice [c,d,**], Carlos Lopez-Larrea [a,b,f]

[a] Translational Immunology, Health Research Institute of the Principality of Asturias (ISPA), Avenida de Roma S/N, Oviedo, Asturias 33011, Spain
[b] ISCIII RICORS2040 Kidney Disease Research Network, Madrid, Spain
[c] Nanobiotechnology for Life Sciences Laboratory, Department of Chemistry in Pharmaceutical Sciences, Faculty of Pharmacy, Universidad Complutense de Madrid (UCM), Plaza Ramón y Cajal s/n, Madrid E-28040, Spain
[d] Microscopy and Dynamic Imaging Unit, Fundación Centro Nacional de Investigaciones Cardiovasculares Carlos III (CNIC), Calle Melchor Fernández Almagro 3, Madrid E-28029, Spain
[e] Atrys Health, Madrid E-28001, Spain
[f] Department of Immunology, Hospital Universitario Central de Asturias, Oviedo 33011, Spain
[g] Health Research Institute of the Principality of Asturias (ISPA), Avenida de Roma S/N, Oviedo, Asturias 33011, Spain
[h] Department of Pathology, Hospital Universitario Central de Asturias, Oviedo 33001, Spain
[i] Biobank of Principality of Asturias, Oviedo 33011, Spain
[j] Lipids in Human Pathology, Institut d'Investigació Sanitària Illes Balears (IdISBa), Ctra. Valldemossa 79, Palma, Balearic Islands E-07120, Spain
[k] Research Unit, University Hospital Son Espases, Ctra. Valldemossa79, Palma, Balearic Islands E-07120, Spain
[l] Department of Nephrology, Hospital Universitario Central de Asturias, Oviedo 33001, Spain

ARTICLE INFO

Keywords:
AKI
ischemia reperfusion injury
BRD4
JQ1
nanobiotechnology
kidney drug delivery

ABSTRACT

Targeting epigenetic mechanisms has emerged as a potential therapeutic approach for the treatment of kidney diseases. Specifically, inhibiting the bromodomain and extra-terminal (BET) domain proteins using the small molecule inhibitor JQ1 has shown promise in preclinical models of acute kidney injury (AKI) and chronic kidney disease (CKD). However, its clinical translation faces challenges due to issues with poor pharmacokinetics and side effects. Here, we developed engineered liposomes loaded with JQ1 with the aim of enhancing kidney drug delivery and reducing the required minimum effective dose by leveraging cargo protection. These liposomes efficiently encapsulated JQ1 in both the membrane and core, demonstrating superior therapeutic efficacy compared to freely delivered JQ1 in a mouse model of kidney ischemia-reperfusion injury. JQ1-loaded liposomes (JQ1-NPs) effectively targeted the kidneys and only one administration, one-hour after injury, was enough to decrease the immune cell (neutrophils and monocytes) infiltration to the kidney—an early and pivotal step to prevent damage progression. By inhibiting BRD4, JQ1-NPs suppress the transcription of pro-inflammatory genes,

Abbreviations: α-SMA, alpha smooth muscle actin; ACN, acetonitrile; AKI, acute kidney disease; AKP, alkaline phosphatase; ALT, alanine aminotransferase; AST, aspartate aminotransferase; BET, bromodomain and extra-terminal; BUN, blood urea nitrogen; CD, cyclodextrin; CKD, chronic kidney disease; DLS, dynamic light scattering; DMPC, 1,2-dimyristoyl-sn-glycero-3-phosphocholine; GGT, gamma-glutamyl transferase; H&E, Hematoxylin & Eosin; HD, hydrodynamic diameter; HPLC, high performance liquid chromatography; IBETs, inhibitors of BET proteins; IEP, isoelectric point; IRI, ischemia-reperfusion injury; MHPC, 1-myristoyl-2-hydroxy-sn-glycero-3-phosphocholine; MRI, magnetic resonance imaging; NPs, nanoparticles; OI, optical imaging; PAS, Periodic acid-Schiff; RdR, rhodamine-red; TEM, transmission electron microscopy.

* Corresponding author at: Translational Immunology, Health Research Institute of the Principality of Asturias (ISPA), Avenida de Roma S/N, Oviedo, Asturias 33011, Spain.

** Corresponding author at: Nanobiotechnology for Life Sciences Laboratory, Department of Chemistry in Pharmaceutical Sciences, Faculty of Pharmacy, Universidad Complutense de Madrid (UCM), Plaza Ramón y Cajal s/n, Madrid E-28040, Spain.

E-mail addresses: beatriz.suarez@ispasturias.es (B. Suarez-Alvarez), mfilice@ucm.es (M. Filice).

[1] These authors contributed equally.

https://doi.org/10.1016/j.biopha.2024.116492
Received 6 January 2024; Received in revised form 12 March 2024; Accepted 19 March 2024
Available online 26 March 2024

such as cytokines (*il-6*) and chemokines (*ccl2, ccl5*). This success not only improved early the kidney function, as evidenced by decreased serum levels of BUN and creatinine in JQ1-NPs-treated mice, along with reduced tissue expression of the damage marker, NGAL, but also halted the production of extracellular matrix proteins (Fsp-1, Fn-1, α-SMA and Col1a1) and the fibrosis development. In summary, this work presents a promising nano-therapeutic strategy for AKI treatment and its progression and provides new insights into renal drug delivery.

1. Introduction

Acute kidney injury (AKI) is a pathology characterised by an abrupt decline of the glomerular filtration rate appearing from a few hours and up to 7 days from injury onset [1]. Major causes of AKI include renal ischemia, sepsis, and nephrotoxicity, which can lead to acute tubular necrosis [2]. Despite medical progress, AKI still leads to substantial morbidity and mortality [3] and, due to kidney maladaptive repair mechanisms, an increased risk of progression of chronic kidney disease (CKD) in survivors [4,5]. Maladaptive repair is thought to be driven by different factors, including persistent inflammation, oxidative stress, and dysregulated signalling pathways, ultimately causing progressive decline of kidney function [6,7]. Unfortunately, currently there are no available therapies to either treat AKI or reduce post-AKI sequelae and CKD progression.

Research has elucidated key mechanisms involved in AKI onset and AKI-to-CKD transition, highlighting the role of epigenetic mechanisms as significant regulators of pathogenesis [8]. The bromodomain and extra-terminal (BET) domain protein family, comprising bromodomain-containing proteins 2, 3, and 4 (BRD2, BRD3, and BRD4) and bromodomain testis-specific protein (BRDT), are epigenetic "readers" able to detect acetylated histones through their bromodomain and recruit the necessary machinery to induce initiation and elongation of transcription [9]. Specifically, BRD4 functions as a transcriptional co-activator involved in regulating various cellular processes such as the cell cycle, inflammatory response, and oxidative stress, making it a target in the pathogenesis of several diseases [10-13]. Recently, our group and others have clarified the role of BRD4 in the development and progression of various kidney diseases. Inhibition of BRD4 diminishes glomerular damage in experimental models of glomerulonephritis [14, 15] as well as podocyte injury in diabetic nephropathy [16], inflammatory renal diseases [17] and kidney fibrosis [18-20], but also improves renal function in AKI experimental models of ischemia-reperfusion injury (IRI) [21] and cisplatin-induced nephrotoxicity [22]. Hence, modulation of BRD4 activity represents a promising target in renal pathology research. However, despite the potential of BET protein inhibitors like JQ1 [23], which has been extensively studied in preclinical models showing promising results in different cancers and autoimmune diseases [24-26], their clinical translation has been hindered by poor pharmacokinetic profiles, low oral bioavailability, and elevated toxicity [27,28]. To address these limitations, there has been a focus on nanotechnology-based approaches, which in general offer advantages such as targeted drug delivery, enhanced biodistribution and pharmacokinetic and reduced toxicity [29].

In this work we investigated the design, synthesis, and characterisation of engineered JQ1-loaded liposomes. The rationale relies on the possibility to selectively concentrate and visualise the highest amount of JQ1 within the kidney thus decrease its minimum effective dose while avoiding the undesired and critical side effects related to the use of JQ1 in its free form. After *in vitro* characterisation, a mouse model of bilateral kidney ischemia-reperfusion injury (IRI) was employed to evaluate the ability of JQ1-NPs to block the initial inflammatory response and loss of renal function and prevent subsequent kidney fibrosis and progression to CKD.

2. Materials and methods

2.1. Synthesis of lipid-based nanoparticles

Three liposome formulations were optimized: liposomes with membrane-encapsulated JQ1 (type I); liposomes with core-encapsulated JQ1 (type II); liposomes with both membrane and core encapsulation (type III or dual encapsulation). In all cases, liposomes were synthesized by the thin lipid film-hydration method. First, stock solutions of lipids were prepared. DMPC was dissolved at 10 mg/mL in chloroform. MHPC and Gd-DTPA-BSA were dissolved at 10 mg/mL in a mixture of chloroform/methanol (3:1 v/v). Liss Rhod PE or Cy 5.5 PE were prepared at 1 mg/mL in chloroform. JQ1 was dissolved in acetonitrile (ACN) in a 5 mg/mL concentration. Then, proper volumes of these stock solutions were mixed to achieve the desired liposome composition. In general, for the three types of liposomes, DMPC, MHPC and Gd-DTPA-BSA lipids were mixed in a molar ratio of 7.6:1.1:1. JQ1 was added (with lipids for type I; with aqueous phase for hydration for type II; and in both cases for type III) in a weight ratio of 1:30 with the total amount of lipids (e. g. for a type I synthesis, 100 μg of JQ1 are offered to 2.8 mg of lipids). The aqueous solution for hydration was added in a proportion of 1 mL H_2O for 2.5 mg of lipids. When a fluorescent probe is needed, Liss Rhod PE or Cy 5.5 PE are added in lipid mixture in a 0.2% of the total lipid mol amount. For nucleus encapsulation of JQ1, cyclodextrin (CD)-JQ1 complex was produced by mixing CD 1% in H_2O with JQ1 5 mg/mL in Acetonitrile in a volume ratio (CD:JQ1) of 9:1, and the complex is then added to the distilled H_2O used for film hydration step.

In more details, for type I liposomes, the solvent of the lipid and JQ1 mixture was evaporated under reduced pressure to form the thin film and then it was hydrated with distilled H_2O, and the solution was sonicated for 1 h at 60°C. For type II liposomes, the solvent of the lipid mixture was evaporated under reduced pressure to form the thin film, and then hydrated with distilled H_2O containing CD-JQ1 complex and sonicated for 1 h at 60°C. For type III liposomes, the solvent of the lipid and JQ1 mixture was evaporated under reduced pressure to form the thin film and then it was hydrated with distilled H_2O containing CD-JQ1 complex and sonicated for 1 h at 60°C. Finally, all samples were centrifuged in Amicon concentrators of 100 kDa molecular weight cut-off (MWCO) at 2900 g for 10 minutes, and washed three times with distilled H_2O, to remove uncomplexed lipids and non-encapsulated drug.

1,2-dimyristoyl-sn-glycero-3-phosphocholine (DMPC), 1-myristoyl-2-hydroxy-sn-glycero-3-phosphocholine (MHPC), DTPA-bis (stearylamide) (gadolinium salt) (Gd-DTPA-BSA), 1,2-dioleoyl-sn-glycero-3-phosphoethanolamine-N-(lissamine rhodamine B sulfonyl) (ammonium salt) (Liss Rhod PE) and 1,2-distearoyl-sn-glycero-3-phosphoethanolamine-N-(Cyanine 5.5) (Cy 5.5 PE) were purchased from Avanti Polar Lipids (Birmingham, UK). (2-Hydroxypropyl)-β-cyclodextrin (CD), iron (III) chloride hexahydrate ($FeCl_3{\cdot}6\ H_2O$) and ammonium thiocyanate (NH_4SCN) were purchased from Merck (Darmstadt, Germany).

2.2. Determination of liposome concentration (Stewart test)

For the determination of liposome concentration, the Stewart test (a colorimetric method based on the complex formation between ammonium ferrothiocyanate and phospholipids) has been used. Briefly, ammonium ferrothiocyanate was prepared dissolving 27.03 g of

$FeCl_3 \cdot 6\ H_2O$ and 30.4 g of NH_4SCN in 1 L of distilled H_2O. To perform the test, after their drying in oven at 50°C overnight, samples were dissolved in the same volume with chloroform, mixed with ammonium ferrothiocyanate in a 1:1 (v/v) ratio, and gently shaked in a vortex for 1 minute. Then it was centrifugated at 1000 rpm for 10 minutes to perform phase separation, and following centrifugation the lower chloroform phase was removed and measured in a spectrophotometer at 488 nm. The lipid concentration of the unknown sample was extrapolated by means of a proper calibration curve previously prepared by analyzing with this assay known concentrations of the same lipids.

2.3. Determination of encapsulation efficiency (HPLC)

The encapsulation efficiency of JQ1 within liposomes was measured by high performance liquid chromatography (HPLC) using a LC-4000 HPLC system equipped with a Diode-array detector (MD-4010) and a column oven (CO-4061) (JASCO, USA). For each preparation, a sample volume of 50 μL was evaporated at 50 ºC and then rehydrated in the same volume with the mobile phase (80% acetonitrile and 20% H_2O milliQ). Sample was analyzed using a Gemini RP-C18 column (250 ×4.6 mm, 5 μm, Phenomenex) with a flow rate of 1 mL/min and a column temperature of 25°C. The mobile phase was 80% acetonitrile and 20% H_2O milliQ, the wavelength was set to 254 nm and the retention time of JQ1 was about 5.4 min. Each prepared sample was quantified by extrapolation with a calibration curve (R^2: 0.991) prepared by using a commercial standard reference of target drug. Each sample was analyzed in triplicate.

2.4. Physicochemical characterization

First, the morphology of prepared liposomes was examined by transmission electron microscopy (TEM) (JEOL JEM 1400). Aqueous colloidal suspensions of liposomes samples were dropped on 200 mesh copper grids coated with formvar/carbon and stained with 1% (w/v) of uranyl acetate. Briefly, sample was placed on grids during 1 min, then washed with H_2O during 30 sec and then stained with uranyl acetate during 1 min. Then the obtained micrographs were analyzed using the program ImageJ, measuring about a total of 200 NPs and examining their size and distribution in Origin.

Measurements of liposomes hydrodynamic size and surface zeta potential were performed on freshly prepared and purified samples using a DLS Zetasizer Nano Zen 3600 (Malvern Instruments, Malvern, UK). For the particle hydrodynamic size analysis, each sample was diluted to the appropriate concentration with filtered distilled water. And for the ζ−potential and isoelectric point analysis, samples were diluted in potassium nitrate (KNO_3, 0.01 M) and the different pH values were set by adding diluted HNO_3 or KOH as acid or base, respectively.

2.5. In vitro fluorescent imaging

Fluorescence *in vitro* imaging of phantom samples was performed with IVIS Imaging System 200 series (Xenogen®) with the following acquisition parameters: DsRed ex/em filter, high level, BIN-HR, FOV: 13.3, f8. These parameters were used for all the concentrations studied.

2.6. Relaxivity measurements and in vitro magnetic resonance imaging

For the final sample prepared, six different dilutions of the initial concentration of gadolinium-based lipids calculated by Inductively Coupled Plasma (ICP) were prepared in distilled H_2O, and T1 and T2 MR relaxation times were measured using a Minispec MQ-60 system (Bruker) operating at 20 mHz. T1 values were acquired in triplicate with a saturation−recovery sequence of 12 exponentially distributed repetition times ranging from 3000 ms to 22 s, whereas T2 values were acquired 3 times, using a CPMG sequence of 3600 points with an interpulse delay of 0.1–1 ms. After measurement of the relaxation times (T1 and T2) for the series of five dilutions for each sample, the corresponding relaxation rates, $R_1 = 1/T1$ and $R_2 = 1/T2$, were calculated and plotted versus the total concentration of lipids in each sample. Those plots were fitted to linear regressions, corresponding the slope of each plot (r_1 and r_2) to the respective ionic relaxivity of the sample under study. After that, magnetic resonance imaging (MRI) studies were performed at BioImaC (ICTS BioImagen Complutense), node of the ICTS ReDIB (https://www.redib.net/) using 1 Tesla benchtop MRI scanner (ICON 1 T-MRI; Bruker BioSpin GmbH, Ettlingen, Germany). ICON 1 T-MRI is a permanent magnet with a gradient system capable of supply 450 mT/m gradient strength. A linear polarized solenoid RF-coil (inner diameter 61 ×52 mm 2 and length 90 mm) was employed. MRI data were acquired using the software package Paravision 6.0.1 (Bruker, BioSpin). The main MRI protocol consisted of two dimensional T1 weighted experiment (T1WI). T1WI coronal anatomical sections were acquired using a spin echo sequence with a repetition time = 750 ms, echo time = 7.5 ms, number of averages = 1, field of view = 35 × 11 mm^2, slice thickness = 1.5 mm and number of slices = 5. The acquired matrix size was 350 × 110 (resolution 0.200 ×0.200 ×1.50 mm) and the total acquisition time ~ 1 minute.

2.7. Mice

All mice used in this study are wild-type and had a C57BL/6 N background (Janvier Labs). Male aged 8–10 weeks were used and acclimatized for 1 week before the study. All animal experiments were approved by the Committee for Animal Experimentation of the Universidad de Oviedo (Spain) and performed in accordance with the European and Spanish legislative and regulatory guidelines (European convention ETS 123, on the use and protection of vertebrate mammals in experimentation and for other scientific purposes, and Spanish Law 6/2013, and R.D. 53/2013 on the protection and use of animals in scientific research), making every effort to minimize mouse discomfort.

2.8. Cell culture and treatments

Human proximal tubular epithelial cells (HK-2 cell line; CRL-2190; ATCC, VA) were cultured in RPMI 1640 medium (Gibco, Carlsbad, CA, USA) supplemented with 10% fetal bovine serum, 1% penicillin/streptomycin, 1% insulin transferrin selenite (Gibco) and 5 ng/mL hydrocortisone (Sigma-Aldrich, St. Louis, MO, USA) and maintained in a humidified incubator at 37°C in an atmosphere of 5% CO_2. The cell passage number used ranged between 20 and 25. The inhibitor JQ1 (+) (supplied by James Bradner's laboratory from Dana-Farber Cancer Institute, Boston, MA, USA) or its inactive enantiomer JQ1 (-) (Selleckchem, Houston, TX, USA) were used for 24 h at concentrations raging 50–500 nM. The same conditions were used for encapsulated JQ1 (JQ1-NPs) cell treatments, and the amount of empty NPs (NPs w/o JQ1) was estimated from the quantification of lipids that the JQ1-NPs had for each drug concentration in order to add to the cells the same lipid concentrations. To analyze NPs cell internalization, rhodamine-red (RdR) labelled JQ1-NPs were added to HK-2 cell cultures for the indicated times (1,3,6,18 and 24 h) at a fixed concentration of 500 nM of JQ1. RdR positive cells were detected on a Gallios Flow Cytometer (Beckman Coulter, Inc.) in the FL2 channel.

2.9. MTT assay

HK-2 cells were seeded in triplicate in a 96-well plate at a density of 10^4 cells/well. Following overnight adherence, the media was replaced with a fresh medium containing the treatments that were added for 24 h. After incubation, media was decanted and the cells were then rinsed twice with PBS. The cells were subsequently incubated for additional 4 hours with 100 μL of freshly prepared MTT (3-(4,5-dimethylthiazol-2-yl)-2,5-diphenyltetrazolium bromide) at 0.5 mg/mL in FBS-free RPMI media at 37°C. Then the supernatant was removed and the formed

formazan crystals were dissolved using 100 μL of DMSO, and cell viability was determined by measuring absorbance at 570 nm using a spectrophotometer (EZ Read 2000 microplate reader, Biochrom).

2.10. Annexin V/7AAD assay

Apoptotic and dead cells were quantified using the FITC Annexin V apoptosis detection kit and 7-AAD (Biolegend), following the manufacturer's instructions. HK-2 cells were plated in 6-well plates at a seeding density of 3×10^6cells/well and after overnight adherence treatments were added for 24 h. Next, supernatants were collected and adherent cells were detached using TrypLE Express Enzyme (ThermoFischer Scientifc) and stained using the FITC-Annexin V Apoptosis detection kit with 7AAD (Biolegend), following the manufacturer's instructions. Fluorescence was analyzed on a Gallios Flow Cytometer (Beckman Coulter, Inc.). Early apoptotic cells were considered as Annexin V+ 7AAD- and late apoptotic/necrotic cells as Annexin V+ 7AAD+.

2.11. Bilateral ischemia-reperfusion injury animal model

Briefly, after induction of anesthesia with 3.5% of inhaled oxygenated isoflurane, the animal was transferred to a heat pad and maintained with 1.5–2% of isoflurane concentration for the rest of the procedure. Before surgery, a bolus of 0.1 mg/kg of buprenorphine was subcutaneously administered to help to reach the anesthetic plane and prevent animal discomfort. Bilateral ischemia reperfusion injury (bIRI) was induced by clamping both renal pedicles for 45 or 30 min (depending on the experimental set) at 37°C, adopting a dorsal approach. After removing the clamps (Micro Serrefines item no. 18055–04, F.S.T., Heidelberg, Germany), reperfusion was verified by visual inspection of the kidney. Sham group mice underwent the same procedure except the renal pedicles were not clamped. For *in vivo* administration of non-encapsulated JQ1, the drug first dissolved in DMSO and subsequently mixed with 10% hydroxypropyl-β-cyclodextrin (Sigma Aldrich) to improve solubility. Vehicle-treated mice were injected with the equivalent volume of DMSO mixed with 10% hydroxypropyl-β-cyclodextrin. Mice were administered a single intraperitoneal injection of free JQ1 at 40 mg/kg, JQ1-NPs at the indicated doses or the required controls (vehicle and NPs w/o JQ1) 1 h after surgery. After 24 h reperfusion, mice were euthanized, and the kidneys and blood collected for further analysis. When operated, mice were individualized to prevent suture pullout and/or infection.

2.12. In vivo imaging system (IVIS)

To assess tissue distribution of JQ1-NPs, sham surgery control mice or bIRI operated mice were anesthetized with isofluorane and intraperitoneally injected with Cy 5.5-conjugated NPs 1 hour after reperfusion or the equivalent time in sham control mice. Images were taken at 1,3,6 and 24 h post-injection by the IVIS Spectrum imaging system (IVIS® Lumina III Series, PerkinElmer, MA). At 24 h organs were excised and imaged separately to perform precise quantification of epifluorescence in terms of efficiency (fluorescent emission normalized to the incident excitation intensity) using the living imaging software version 3.2 (Caliper LifeSciences, MA, USA) and Aura Imaging Software (v4.0, Spectral Instruments Imaging, AZ, USA,). The following acquisition parameters were used: 640ex/em filter, lamp level high, binning factor:2, FOV: 12.5, f4 (for mice) and f16 (for organs).

2.13. RNA extraction and real-time quantitative PCR

Total RNA from HK-2 cells or frozen kidneys was isolated using a GeneMATRIX Universal RNA purification kit (EURx, Gdansk, Poland) following the manufacturer's instructions. Purified RNA (1000 ng) was reversed-transcribed to cDNA using a high-capacity cDNA reverse-transcription kit (Applied Biosystems, Foster City, CA, USA). Quantification was performed by the reverse transcription-polymerase chain reaction (RT-PCR) using TB Green Premix Ex Taq II (Takara Bio Inc., Kusatsu, Japan) or TaqMan Gene Expression Master Mix (Applied Biosystems) and analyzed with a StepOnePlusTM Real-Time PCR System (Applied Biosystems). Gene-specific primers used are listed in Supplementary Table 4. Expression of each gene of interest was normalized to the housekeeping gene *Gapdh*. Data were calculated by the ΔCt method.

2.14. Histology

Kidney and liver samples were fixed in 4% formaldehyde and embedded in paraffin using routine methods. When required, slices (5 μm) were stained with Hematoxylin & Eosin (H&E) and/or Periodic acid-Schiff (PAS) stainings. The later was used for pathological injury estimation, after analysis by a pathologist in a blind procedure. A minimum of 10 fields for each kidney slide were examined and scored for pathological injury. A score from 0 to 4 was given for pathological assessment: 0, normal histology; 1, mild injury, 5–25% of tubules showed pathological damage; 2, moderate injury, 25–50% of tubules showed pathological damage; 3, severe injury, 50–75% showed pathological damage; and 4, almost all tubules in field of view were damaged. The average histological score for each sample was calculated. For direct visualization of collagen fibers and histological assessment of collagen deposition, trichrome staining was performed using the Masson Trichrome Staining Kit following manufacturer's instructions (Bio-optica, Milan, IT). Images were acquired with an optical microscope (DM2500; Leica) equipped with a CCD camera (DFC420; Leica), with Leica Application Suite software (version 4.3.0).

2.15. Assessments of biochemical parameters

Blood samples were collected by cardiac puncture from isofluranesedated mice and allowed to clot by leaving it undisturbed at room temperature for 30 minutes to 1 hour. Then samples were centrifuge at 13,000 rpm for 10 minutes at 4ºC and the serum layer transferred to clean tubes and stored at −80ºC until further use. Serum creatinine and urea were determined using a creatinine assay kit (ab204537, Abcam, Cambridge, UK) and a blood urea nitrogen (BUN) colorimetric detection kit (K024-H5, Arbor Assays, MI, USA), respectively, and according to the manufacturer's instructions. The liver enzymes alanine aminotransferase (ALT), aspartate aminotransferase (AST), gamma-glutamyl transferase (GGT) and alkaline phosphatase (AKP) were determined using the Siemens Dimension RXL MAX HM Chemistry Analyzer (Siemens Healthcare Diagnostics Gmbh, Marburg, Germany) in accordance with the manufacturer's instructions.

2.16. Western blot

Total kidney proteins were extracted using RIPA lysis buffer supplemented with a protease and phosphatase inhibitor cocktail (Merck Millipore, Burlington, MA, USA) by mechanically disrupting the tissue with an electric tissue homogenizer (T-10 basic ULTRA-TURRAX, IKA, Germany) and let for 30 min on ice. Then samples were sonicated, centrifuged, and quantified using the Bradford protein assay (Bio-Rad) following separation on 10–12% polyacrylamide-SDS gels. Membranes were incubated overnight at 4°C with the following primary antibodies: NGAL (sc-515876, 1:500; Santa Cruz Biotechnology, Santa Cruz, CA, USA), KIM-1 (AF1817, 1:1000; R&D Systems), α-SMA (ab242395, 1:1000; Abcam), Fibronectin (ab2413, 1:1000; Abcam) and β-actin (sc-47778, 1:2000; Santa Cruz Biotechnology, CA, USA); followed by incubation with HRP-conjugated IgG secondary antibody for 1 h. Immunostained bands were visualized using a chemiluminescence kit (Luminata Forte Western HRP Substrate; Merck Millipore), detected on a system ImageLab (Bio-Rad, Hercules, CA, USA) and quantified with ImageJ version 1.53k software (NIH). Original uncropped WB images

are shown in Supplementary Figure 7.

2.17. Flow cytometry analysis of kidney immune cell infiltration

Kidneys were minced in small pieces and digested with 0.2 mg/mL Liberase TM (Roche) and 40 µg/mL DNAseI (Roche) diluted in RPMI medium without serum for 30 min at 37°C in constant agitation. At the end of the incubation period, enzyme activity was blocked by adding 50 mL PBS supplemented with 0.2% FBS and 0.05 mM EDTA, and the sample was mechanically disrupted by passing through a 70-µm cell strainer to obtain a cell suspension. Before all staining procedures, kidney cell suspensions were incubated with anti-mouse FcRII/III (clone 2.4G2, TONBO Biosciences) and Zombie Red Fixable Viability Dye (Biolegend) for 20 min at 4°C in PBS without serum. Flow cytometry analysis of bIRI-induced inflammation was performed with anti-mouse antibodies to the following antigens: CD45, CD11b, F4/80, Ly6G, Ly6C (TONBO Biosciences). Absolute cell numbers were obtained using TruCount Tubes (BD Biosciences). Cell samples were acquired in a spectral flow cytometer (Northern Lights 3 L, Cytek Biosciences), and the data were analyzed with FlowJo software (v10.8.1, BD Biosciences).

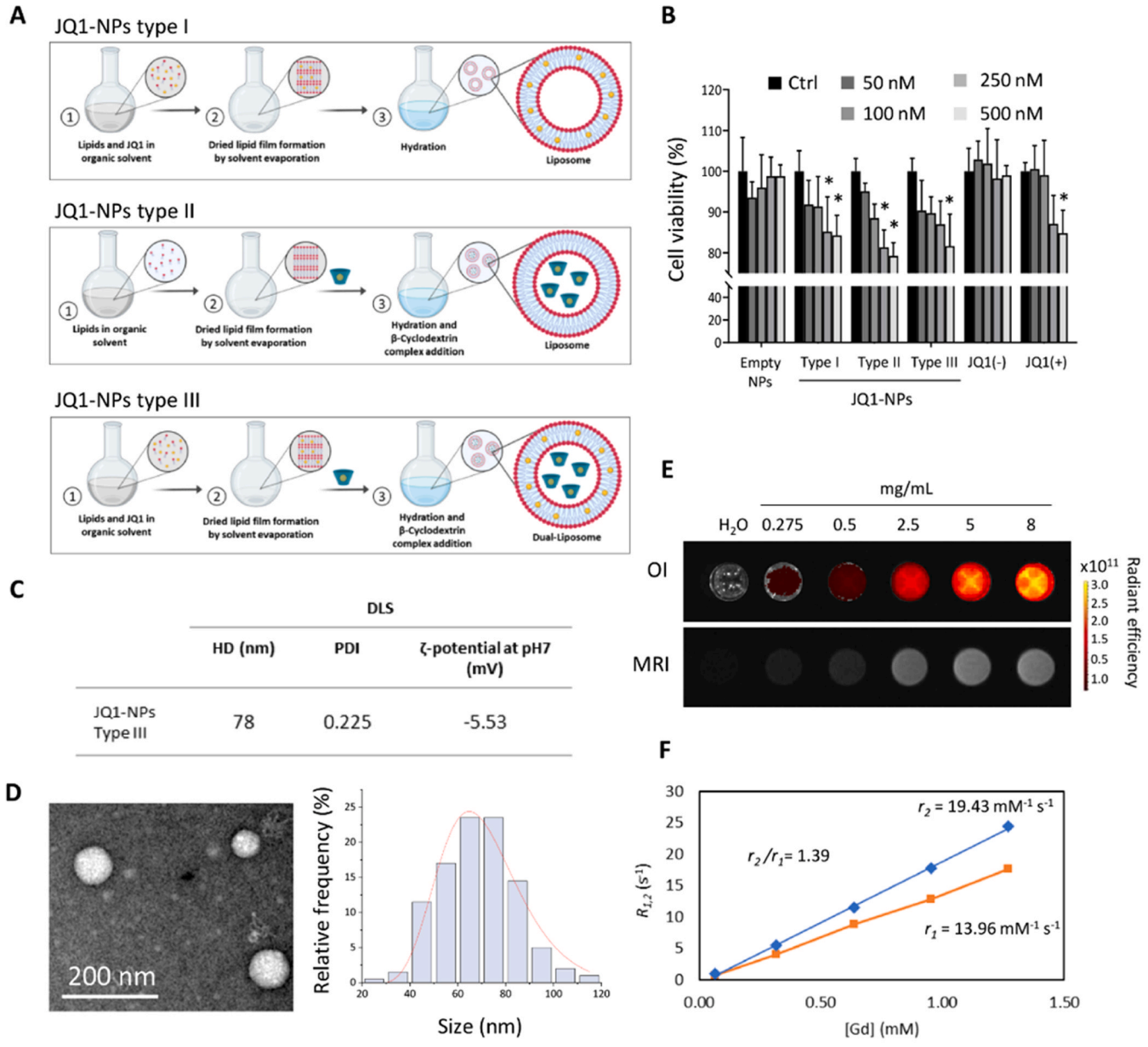

Fig. 1. Synthesis and characterisation of JQ1 liposomal nanoparticles. (A) Schematic representation of type I liposomes (I), type II liposomes (II), and type III liposomes (III) procedure of synthesis. (B) Viability of HK-2 cells determined using the MTT assay. Cells were treated with unencapsulated JQ1 (+) or its inactive enantiomer JQ1 (-), or with JQ1 (+) encapsulated in types I to III liposome nanoparticles (NPs). Empty NPs were used to assess NP- and JQ1-independent toxicities. Results are expressed as a percentage of the control cells (untreated, *black bars*). Data are presented as mean ± standard deviation of n = 4 replicates (wells) per group and are representative of three independent experiments. Statistical analysis was performed using two-way ANOVA followed by Tukey's multiple comparison test. *p<0.05, compared to each control (*black bars*). Ctrl, control. (C) Hydrodynamic diameter (HD) and surface ζ -potential at pH 7 of JQ1-NPs type III liposomes analysed by dynamic light scattering (DLS). PDI, polydispersity index. (D) Transmission electron microscope (TEM) micrograph of JQ1 type III liposomes (*left*) and average size distribution of type III JQ1-NPs analysed by TEM (n=200) (*right*). (E) Fluorescence emission spectrum after excitation with DsRed ex/em filter and T_1-weighted MRI phantom images. OI, optical imaging. MRI, magnetic resonance imaging. (F) Plots of T_1 and T_2 relaxation times as a function of gadolinium (Gd) concentration.

2.18. Hematological analysis

Mice were IP administered NPs-JQ1 at a dose of 40 mg/kg and blood samples analyzed at day 1, 7 and 14 afterwards. Blood samples were obtained after cardiac puncture extraction and collected into EDTA anticoagulant tubes. The automated Element HT5 Hematology Analyzer (Heska, Canada) was used following manufacturer's instructions.

2.19. Statistical analysis

Data were summarized as the mean ± standard deviation (SD) of at least two independent experiments. Normal data distribution was assessed with the Kolmogorov Smirnov test, and the statistical significance of between-group differences was assessed by one-tailed unpaired Student's t-test or one-way ANOVA with Newman–Keuls multiple comparison t-test, as required. All statistical analyses were performed with GraphPad Prism (GraphPad Software Inc. v8.0, San Diego, CA, USA). Statistical significance was concluded for values of $p<0.05$. Statistical details of the experiments and significance are noted in the respective figures and legends.

3. Results

3.1. Optimizing JQ1 loading in liposomal nanocarriers

The methodology for liposome preparation was refined to achieve maximum encapsulation of JQ1 while maintaining its colloidal and physicochemical properties. For this, different synthesis protocols, lipid mixtures, and drug:lipid ratios were tested. As a first approach, considering the hydrophobic nature of JQ1, we studied its encapsulation within the membrane (JQ1-NPs type I, Fig. 1A) and compared 18-carbon chain (DSPC:PC:Gd-DTPA-BSA) *vs* 14-carbon chain (DMPC:MHPC:Gd-DTPA-BSA) lipid mixtures with a JQ1:lipid molar ratio of 1:50. In general, JQ1 encapsulation performed better in the membrane of lipids with shorter carbon chains (C14), which permitted a load of about 10 μg of JQ1 per mg of lipid **(Additional table 1:** Table S1). Different combinations of long and short chain lipids plus the addition of adjuvants such as cholesterol were tested, however, encapsulation yields did not increase significantly (Table S1). Based on these results, the DMPC:MHPC:Gd-DTPA-BSA lipid composition was selected and then different JQ1:lipid ratios (1:30, 1:50, and 1:100) were tested. No significant changes in terms of encapsulation efficiency were observed (**Additional table 2:** Table S2) so the 1:30 ratio was used thereafter. Next, encapsulation of JQ1 in the liposome core was optimised (JQ1-NPs type II, Fig. 1A). For this purpose, 1% β-cyclodextrin was used to form an inclusion complex with JQ1 which permitted drug encapsulation within the aqueous nucleus of the liposome. With this strategy, about 17 μg of JQ1 per mg of lipid was loaded. Finally, by applying the conditions previously optimised (JQ1-NPs type I and II), JQ1-NPs type III liposomes were synthesized (Fig. 1A) by encapsulating the drug within both membrane and core of liposomes and a synergistic yield of 35 μg of JQ1 per mg of lipid was achieved.

3.1.1. Physicochemical and imaging properties and in vitro cytotoxicity of JQ1 liposomes

We then assessed how each liposome preparation influenced cell viability using the MTT assay in HK-2 renal tubular epithelial cells. The three NPs types did not show significant differences in terms of cytotoxicity even at the highest JQ1 dose (500 nM) (Fig. 1B). Moreover, no effect was detected either with empty NPs or the non-encapsulated inactive JQ1 enantiomer, indicating that cytotoxicity was inherent to JQ1 itself and not the NPs nor the encapsulation process. Therefore, considering type III liposomes allowed the highest amount of JQ1 encapsulation, studies were continued with this formulation. Moreover, these results were corroborated using the Annexin V/7AAD assay which showed that the percentage of apoptotic and necrotic cells was always <12% (**Additional** Fig. 1**:** Fig. S1).

Liposomes were characterised by dynamic light scattering (DLS) to evaluate the hydrodynamic diameter (HD) and isoelectric point (IEP) of JQ1 liposomes (Fig. 1C) as well as transmission electron microscopy (TEM) to visualise morphology and calculate size distribution (Fig. 1D). By DLS, liposomes showed an average HD of 78 nm and polydispersity index of 0.225 and by TEM they showed a characteristic spherical morphology with an average diameter of 68 ± 6 nm. A pH of 6 was found for the IEP (**Additional** Fig. 2**: Fig.S2**). Therefore, the surface ζ-potential of JQ1 liposomes will be negative at physiological pH (**Additional** Fig. 2**: Fig.S2**). Small size and negative surface ζ-potential at physiological pH represent critical parameters to obtain nanoformulations that are expected to be colloidally stable for *in vivo* kidney targeting. Considering the liposome composition (presence of fluorescent dye and gadolinium salt), the overall potential of JQ1 liposomes to act as contrast agents for multimodal molecular imaging was evaluated *in vitro* using phantom imaging techniques (Fig. 1E). Due to the presence of rhodamine-labelled lipid, fluorescence optical imaging (OI) was assessed by evaluating the contrast generated by increasing concentrations of JQ1 liposomes. Higher NP concentration led to higher fluorescence intensity with good linear correlation (R^2=0.994) in the 0.275–5 mg/mL concentration range. Because of the incorporation of gadolinium salt, magnetic resonance imaging (MRI) was used to assess the potential of JQ1-NPs to modify the relaxivity times of water samples (Fig. 1E). As expected, brighter images were achieved as a function of increasing NP concentration. Relaxivity values of 19.43 mM^{-1} s^{-1} for the transversal r_2 and 13.96 mM^{-1} s^{-1} for the longitudinal r_1 were observed (Fig. 1F), showing an r_2/r_1 ratio of 1.39. Overall, these results indicate that, in addition to therapeutic activity, JQ1-NPs can be used as a multimodal contrast agent for both T_1-weighted MRI and OI molecular imaging modalities.

3.2. Cell uptake of JQ1 liposomes and in vitro functional assays

Since internalisation into the target cell is a prerequisite for the proper activity of the encapsulated drug, NP uptake was evaluated in HK-2 cells. Fluorescent JQ1-NPs were incubated with HK-2 cell cultures for 1, 3, 6, 18, and 24 h at a fixed concentration of 500 nM of JQ1 and analysed by flow cytometry (Fig. 2A). Results showed that there was efficient uptake of JQ1-NPs, and nearly 100% of cells were rhodamine-positive after 24 h (Fig. 2B). Functional experiments were performed at 24 h post-treatment by evaluating gene expression of *IL6* and *CCL2*, two known targets of the JQ1 BET inhibitor, after prior induction with TNF-α. Results showed that, similarly to free JQ1, JQ1-NP treatment led to a decrease in *IL6* (Fig. 2C) and *CCL2* (Fig. 2D) expression in a dose-dependent manner. Thus, this indicates that JQ1 was efficiently released from NPs into target cells exerting its function.

3.3. JQ1-loaded liposomes successfully target the kidney

The *in vivo* effect of JQ1-NPs was assessed in a mouse model of kidney damage induced by bilateral IRI (Fig. 3A). Initially, *in vivo* biodistribution was visualised using Cy 5.5-labelled JQ1-NPs and intraperitoneally administered to mice after 45 min of ischemia or in sham-operated mice. Images were acquired using the IVIS® Imaging System at 1, 3, 6, and 24 h after NP injection. Dorsal images indicated that NPs reach the kidneys at 1 h post-injection and were maintained in the organ up to 24 h (Fig. 3B). However, ventral images showed that NPs spread throughout the entire peritoneum (site of injection) at shorter times (1 and 3 h) but finally concentrated in the upper-medial area, corresponding to the liver, at longer times. No differences were detected between sham or 45 min ischemia at any time, meaning that organ damage did not impact NPs biodistribution (Fig. 3B), a result confirmed by *ex vivo* quantitative analysis of organs harvested after 24 h (Fig. 3C, D). Maximum accumulation of NPs was detected in the liver, pancreas, and kidneys. Results showed that efficient renal uptake of JQ1 liposomes

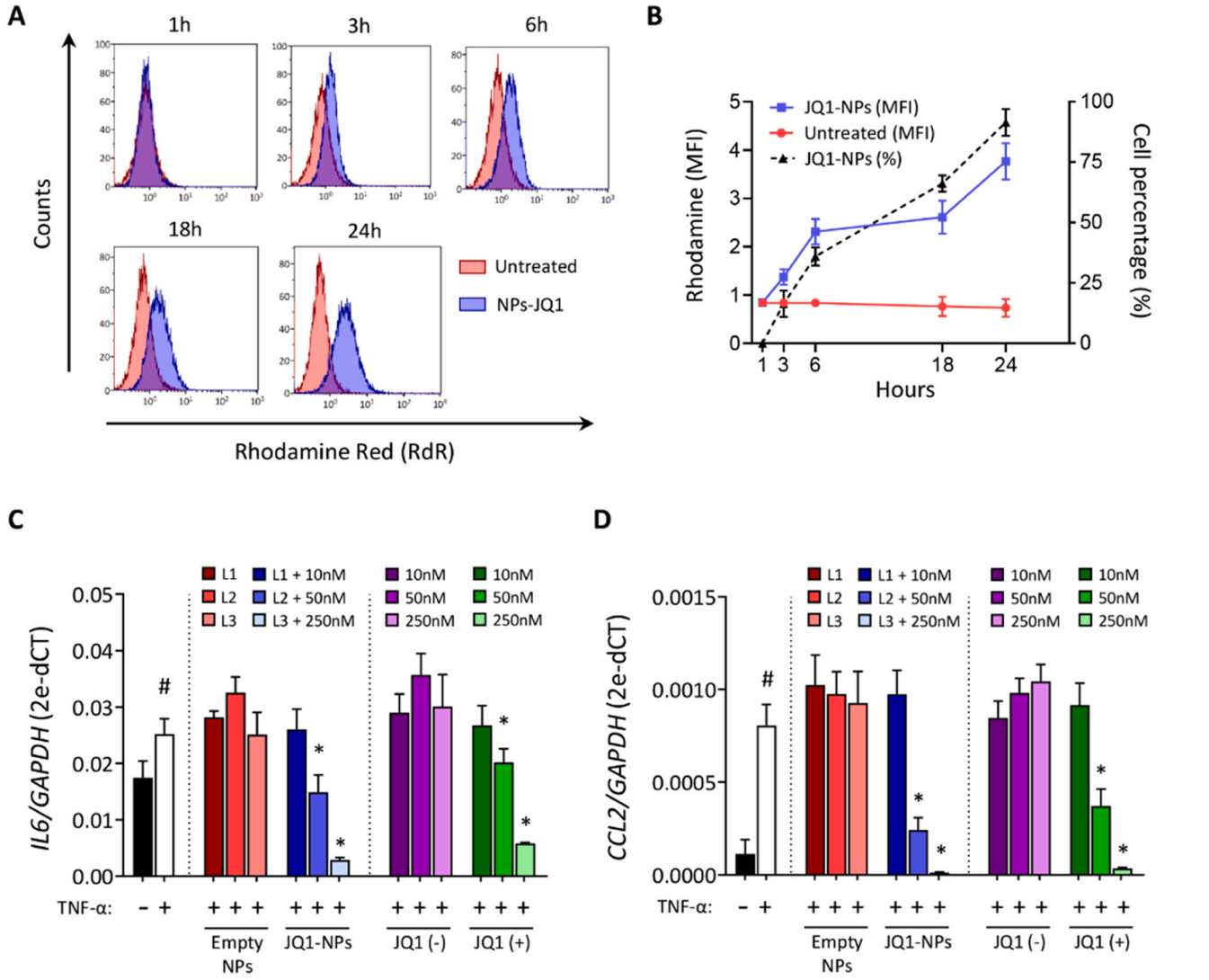

Fig. 2. *In vitro* effectivity of JQ1-loaded nanoparticles (NPs). (A) Representative flow cytometry histograms showing the fluorescent intensity of rhodamine red (RdR) NPs-JQ1 uptake by HK-2 cells (*blue*) compared to control untreated cells (*red*) at 1, 3, 6, 18, and 24 hours. (B) Mean fluorescence intensity (MFI) of RdR-NPs-JQ1 treated (*blue line*) and untreated cells (*red line*) along with the percentage of positive cells (*right Y axis, black dotted line*) are represented at the indicated times. Gene expression levels of *IL6* (C) and *CCL2* (D) were analysed by qPCR in HK-2 cells treated with empty NPs, NPs-JQ1, JQ1 (+), or JQ1 (-) for 24 hours at different doses and TNF-α stimulation (10 ng/mL) for the last 3 hours. L1, L2, and L3 represent the three lipid concentrations (0.5, 2.5, and 25 mM, respectively) used in the NPs-JQ1 treatments for the corresponding 10, 50, and 250 nM doses of JQ1. *GAPDH* was used as a housekeeping gene. For all experiments, error bars represent the mean ± standard deviation of n = 3 per condition and data are representative of three independent experiments. Statistical analysis was performed using two-way ANOVA followed by Tukey's multiple comparison tests. * $p<0.05$, compared to each control (empty vs NPs-JQ1 doses and JQ1 (-) vs JQ1 (+) doses); # $p<0.05$ compared to unstimulated cells.

occurred within hours and was maintained for longer time periods.

3.4. Liposome-mediated JQ1 delivery boosts its effectiveness and reduces renal damage

The effectivity of JQ1-NPs was evaluated after bilateral IRI. Different doses (10, 20, 30, and 40 mg/kg) were administered intraperitoneally 1 h post-ischemia and effects evaluated after 24 h of reperfusion (Fig. 4A). Results showed a significant and dose-dependent reduction of the NGAL (*Lcn2*) kidney damage marker in mice treated with 30 and 40 mg/kg doses of JQ1-NPs (Fig. 4B, C). Similarly, blood urea nitrogen, and creatinine levels were significantly reduced at the highest dose (Fig. 4D, E). Based on these results, the 40 mg/kg dose was selected for subsequent experiments. KIM-1 expression could not be evaluated as a renal damage marker due to its minimal expression at all tested concentrations, even at doses where an improvement of renal function was undetected (**Additional** Fig. 3**:** Fig. S3A**,**B).

To assess the effectiveness of the JQ1 liposome formulation, the experimental design was repeated, but in this case, we use soluble JQ1 at the same dose (40 mg/kg) (Fig. 5A) and results were compared to those obtained with JQ1-NPs under the same conditions (Fig. 4). Soluble JQ1 did not decrease NGAL expression (Fig. 5B, C) to the extent observed with JQ1 liposomes. Accordingly, blood urea nitrogen (Fig. 5D), and creatinine (Fig. 5E) levels did not show differences among the vehicle and soluble JQ1 groups. Moreover, PAS staining showed a marked reduction in tubular necrosis after JQ1-NPs administration in the corticomedullary junction (the most affected area within the kidney after renal IRI) as confirmed by the presence of detached or sloughed tubular cells and loss of brush border (Fig. 5F). Additionally, decreased cast formation (or clusters of cellular debris, proteins, and other biological materials obstructing the tubules; Fig. 5F) was observed. Overall, these results indicate less renal injury in mice treated with JQ1-NPs compared

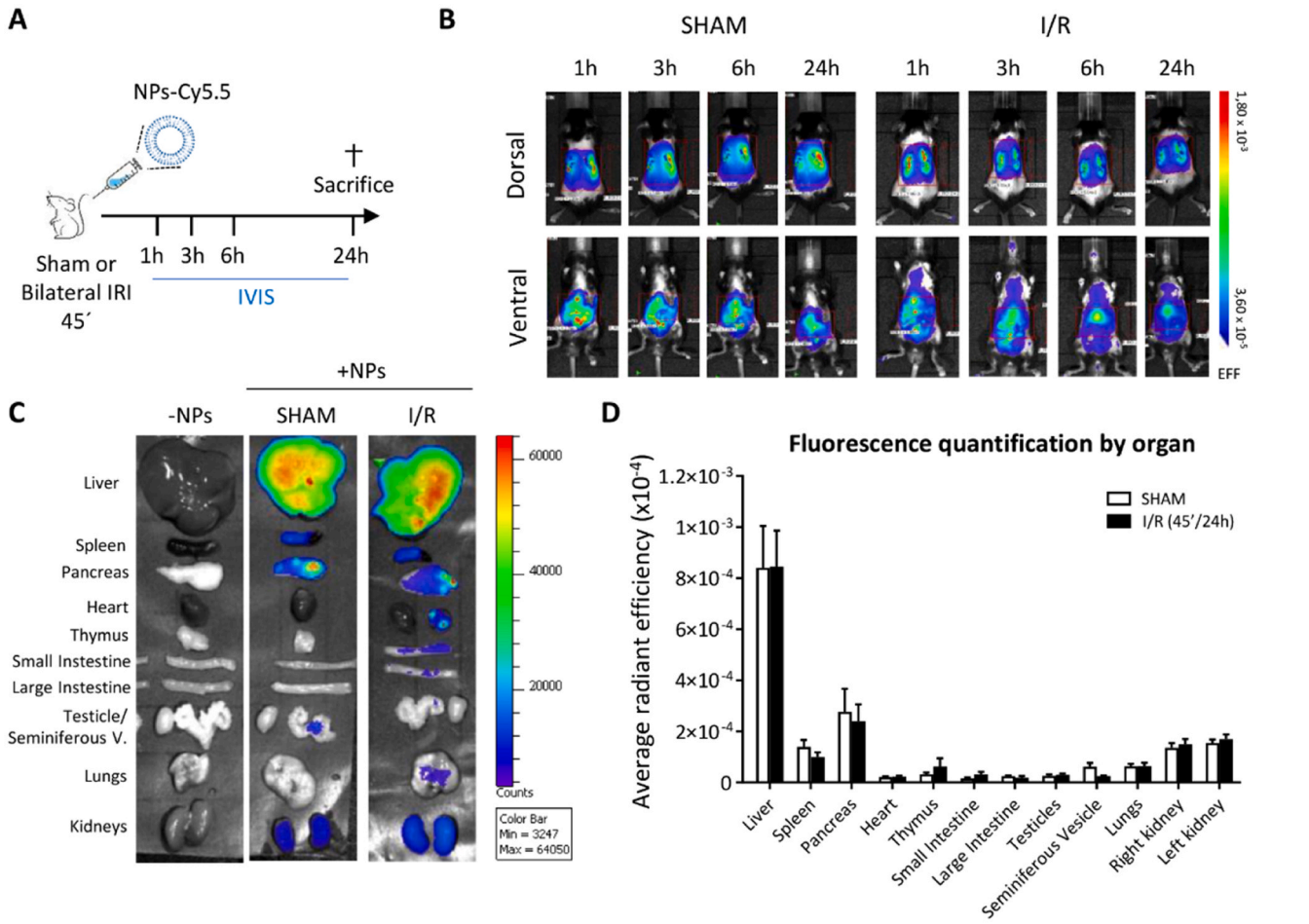

Fig. 3. *In vivo* biodistribution evaluation of fluorescent-labelled nanoparticles (NPs). (A) Cy5.5-conjugated NPs were intraperitoneally injected immediately after the ischaemic insult and images were acquired by an IVIS Lumina III Imaging System at 1, 3,6, and 24 h of reperfusion. (B) Fluorescence signal captured in whole mice from dorsal and ventral positions. Sham (*left*) or ischaemic mice (I/R; *right*) were analysed. (C) *Ex vivo* imaging of isolated organs obtained from sham or ischaemic mice at 24 h post-injection with NPs. (D) Quantitative analysis of NP accumulation in the organs shown in (C). The data are presented as the average radiant efficiency percentage, which is the amount of photons emitted by the sample per unit time, per unit surface area, and exposure time. Data are presented as mean ± standard deviation of n = 3 mice per group. For (B) and (C), representative images are shown. Data are representative of three independent experiments with similar results.

to soluble JQ1.

To evaluate potential reduction in *in vivo* systemic toxicity related to JQ1 encapsulation, serum liver biomarkers and histology were analysed in ischaemic mice. Mice treated with JQ1-NPs presented better liver functionality as confirmed by reduced serum levels of ALT, AST, and AKP enzymes versus soluble JQ1 (**Additional** Fig. 4A: Fig. S4A). Liver histological assessment of the mouse group treated with soluble JQ1 showed higher hepatocyte swelling in comparison with JQ1-NPs-treated mice (**Additional** Fig. 4B:**Fig.S4B**). Administration of JQ1 liposomes (40 mg/kg) to non-ischaemic mice did not impact body weight for up to 14 days (**Additional** Fig. 5:**Fig.S5**). No relevant changes in the blood peripheral subsets were observed within the same time range (**Additional table 3:** Table S3). Overall, these results demonstrate that JQ1 liposomes enhance drug effectiveness while avoiding renal function loss and reducing systemic side effects.

3.5. JQ1-NPs reduce the kidney inflammatory response

In IRI, inflammation becomes excessive and has a critical role in mediating injury responses. Since early targeting of the inflammatory response is crucial to ameliorate kidney damage, the anti-inflammatory potential of JQ1-NPs in comparison to free drug was assessed at 24 h after bilateral IRI (Fig. 6). Results showed that JQ1-NPs lowered the expression level of representative chemokines (*Ccl2*, *Ccl5*, and *Csf2*) and inflammatory cytokine (*Il6*) (Fig. 6A). The presence of neutrophils ($CD45^+CD11b^+Ly6G^{hi}Ly6C^{low}$) and monocytes ($CD45^+CD11b^+Ly6G^-Ly6C^{hi}$ $F4/80^{low}$) was analysed by flow cytometry (**Additional** Fig. 6: Fig. S6). Upon renal injury, an early increase in neutrophil and monocyte cell infiltration was detected within the kidneys, which was significantly reduced in mice treated with JQ1-NPs (Fig. 6B-E). In contrast, no significant differences were detected in the soluble JQ1 mouse group, confirming the enhanced anti-inflammatory activity of JQ1 liposomes.

3.6. Post-ischaemic renal fibrosis progression is halted by JQ1-NPs treatment

Since inflammatory cell infiltration is a key driver of subsequent fibrosis development, we examined whether inhibition of the inflammatory burden at the acute phase of renal damage can preserve long-term organ function. With this aim, a 30 min bilateral IRI was performed since the 45 min ischemia model results in higher lethality at 3–4 days and thus long-term progression cannot be evaluated properly [30]. At 1 h post-ischemia, mice were administered with a single dose of JQ1-NPs (40 mg/kg) and damage was evaluated at day 21 (Fig. 7A). Upon treatment with JQ1 liposomes, reduced expression of profibrotic

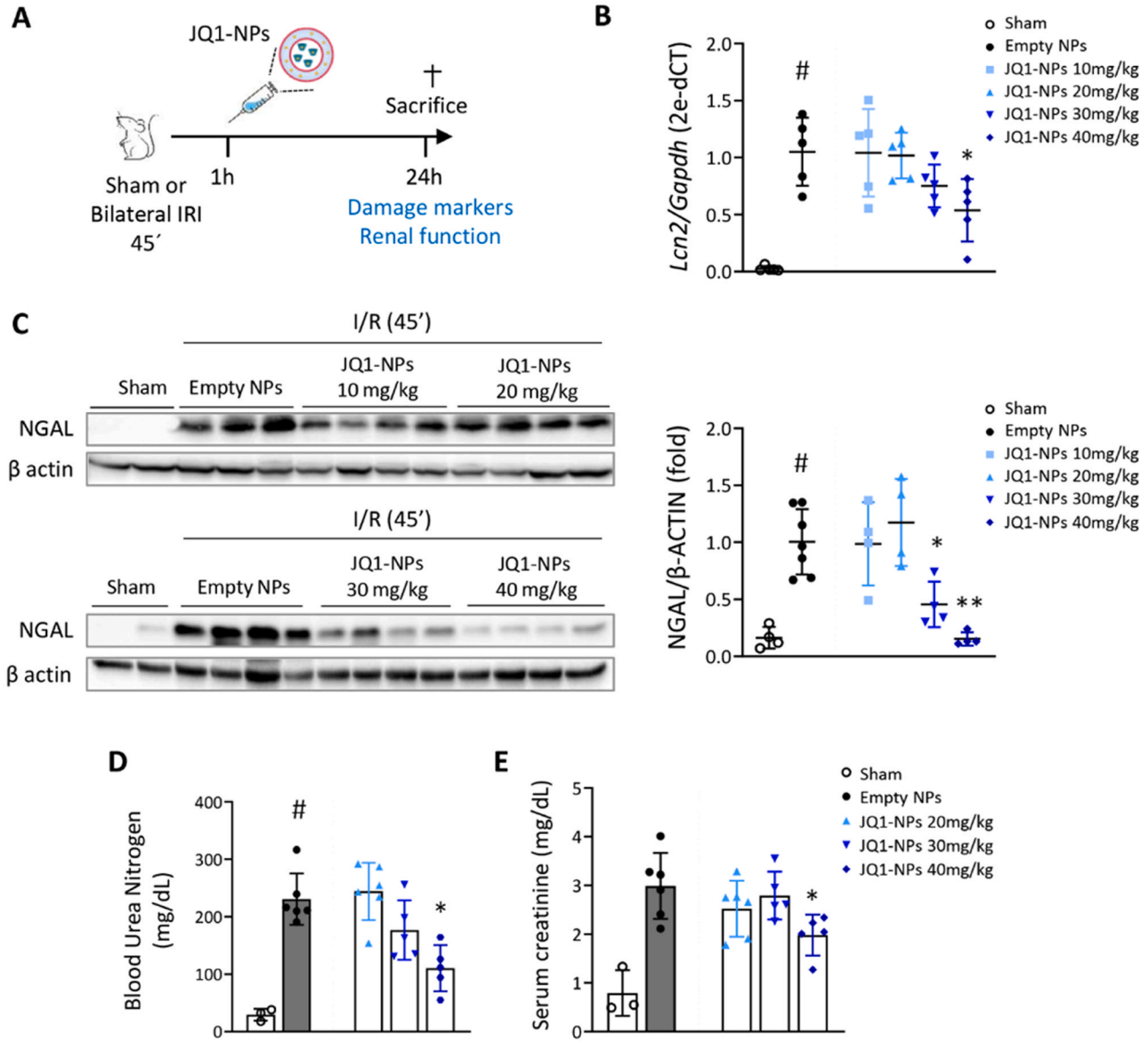

Fig. 4. Mice treatment with JQ1-NPs following bilateral ischemia-reperfusion injury results in decreased kidney damage. (A) Schematic representation of experimental design. A 45 min renal bilateral ischaemic injury was performed followed by administration of NPs-JQ1 at dosages of 10, 20, 30, and 40 mg/kg at 1 h after reperfusion. Mice were sacrificed at 24 h. (B) *Lcn2* (NGAL) gene expression levels were analysed by qPCR and normalised to the empty nanoparticles (NPs) ischaemic group. Sham mice were used as the control group. (C) Levels of renal NGAL protein were assessed by western blotting. Images show the expression levels of 2 (sham) or 4 representative animals per group (*left*). Normalised quantification to the ischaemic group without treatment (empty NPs) is shown (*right*). β-actin was used as the loading control protein. (D) Blood urea nitrogen (BUN; mg/dl) and (E) serum creatinine (mg/dl) levels assessed in mice from the different groups at 24 h post-ischaemic damage in the 20, 30, and 40 mg/kg NPs-JQ1 administered mice. Results are mean ± standard deviation of 3–4 (Sham) to 5–6 (I/R) animals per group. Data are representative of three distinct experiments with comparable results. Statistical analysis was performed using one-way ANOVA and Tukey's multiple comparisons tests. # $p<0.05$ *vs.* Sham; and *$p<0.05$, **$p<0.01$ *vs.* empty NPs damage group.

genes such as fibronectin 1 (*Fn1*), fibroblast-specific protein (*Fsp1*), α-smooth muscle actin (*α-Sma*), and collagen 1α1 (*Col1a1*) was observed (Fig. 7B). Decreased expression of *Fn1* and *α-Sma* was also detected at the protein level (Fig. 7C). Masson's trichrome staining indicated that administration of only one dose of JQ1-NPs was sufficient to reduce the collagen deposits and ameliorate the interstitial fibrosis at day 21 (Fig. 7D). A noticeable decrease of the kidney injury marker NGAL (by qPCR analysis of the *Lcn2* gene) was observed (Fig. 7E). Renal malfunction was improved as demonstrated by decreased serum levels of BUN in JQ1 liposome-treated mice (Fig. 7F).

4. Discussion

In this study a novel approach for preparing engineered multifunctional liposomes loaded with the BET protein inhibitor JQ1 is described for potential use as an advanced therapy for AKI and progression to CKD. Nanoformulation of drugs has demonstrated several benefits, including increased drug stability, targeted delivery, reduced toxicity, and improved pharmacokinetics [31]. These nanocarriers can be engineered to target specific tissues therefore improving the drug bioavailability while reducing its side toxicity [32]. Due to these advantages, the interest in applying nanotechnology to improve therapeutic strategies has increased in recent years [33]. However, the application of nanotechnology for the treatment of renal diseases is still in its infancy [34].

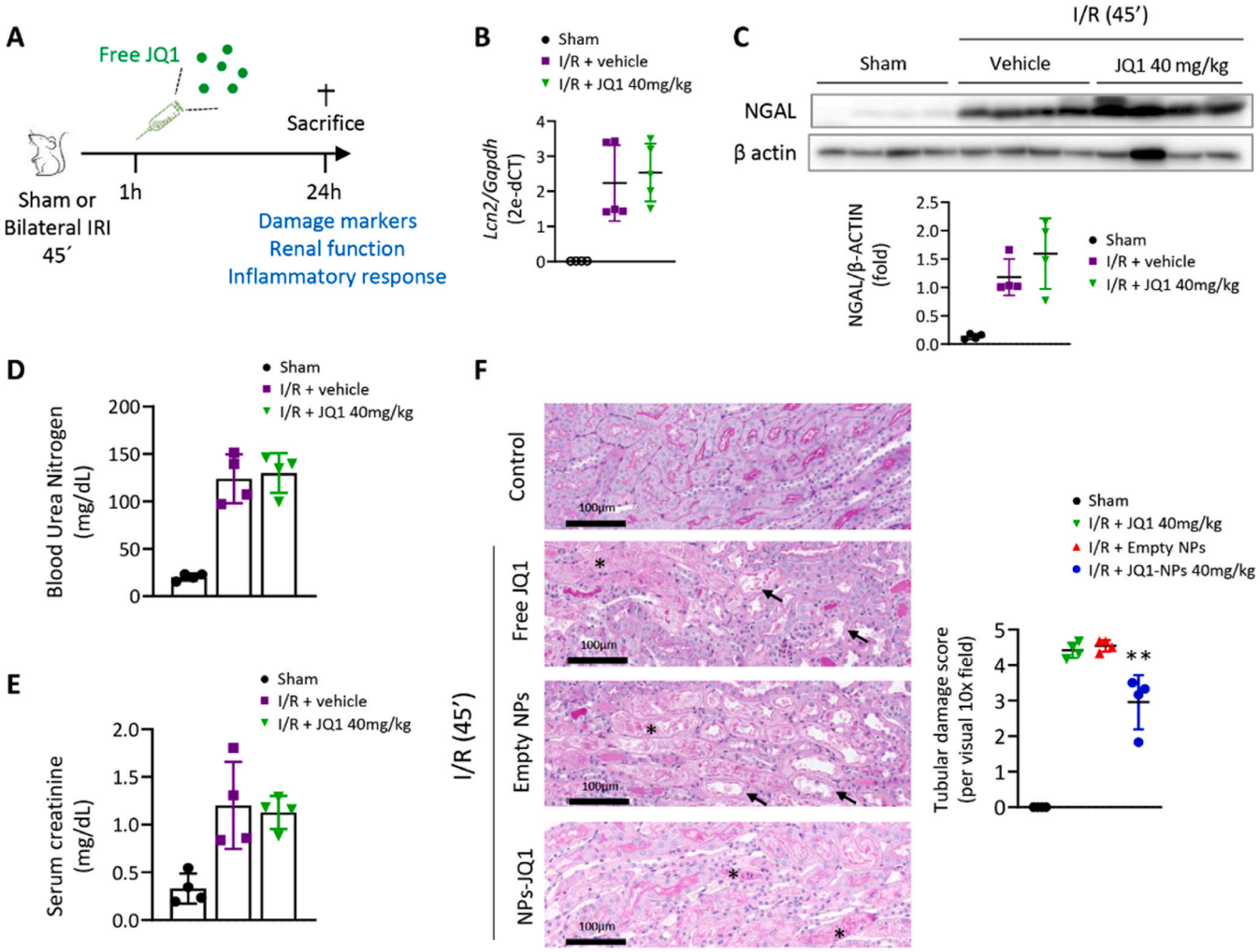

Fig. 5. Equivalent treatment with free JQ1 does not improve renal damage. (A) Schematic representation of experimental design. A 45 min renal bilateral ischaemic injury was performed followed by the administration of the vehicle (DMSO/10% β-cyclodextrin 1:10) or non-encapsulated (free) JQ1 at a unique dose of 40 mg/kg 1 hour after reperfusion. Mice were sacrificed at 24 h. Expression levels of *Lcn2* (NGAL) were quantified by qPCR (B) and protein levels were assayed by western blotting (C) in the vehicle (*purple squares*), free JQ1 (*green triangles*) and control groups. *Gapdh* and β-actin were used as loading controls. Absolute quantification of NGAL from the blots is shown (*below*). (D) Blood urea nitrogen (BUN; mg/dl) and (E) serum creatinine (mg/dl) levels are shown for each analysed group. For all experiments, error bars represent the mean ± standard deviation of n = 4 mice per group and data are representative of three separate experiments. (F) Representative PAS-stained sections for sham and ischaemic animals (I/R) treated with empty nanoparticles (NPs), NPs-JQ1, and unencapsulated (free) JQ1 at a dose of 40 mg/kg. *Asterisks* (*) indicate presence of tubular casts and *arrows* highlight necrotic areas. Scale bar=100 μm.

Therefore, the aim of this study was to enhance the drug efficacy of JQ1 while minimizing side effects by exploiting the advantages offered by nanotechnology and to explore its potential applications in the field of nephrology. Due to its anti-tumoral properties, JQ1 loading in different nanocarriers has previously been studied in oncology [35-37], but not in the field of the nephrology. However, most of the NPs tested were inorganic or polymer-based and did not offer the inherent advantages of liposomes, such as i) high biocompatibility since they are made of phospholipids (i.e., natural compounds found in cell membranes); ii) high synthetic flexibility since they allow encapsulation of both hydrophilic and hydrophobic drugs and wide surface functionalisation; and iii) elevated bloodstream stability which reduces the likelihood of drug degradation or premature release [15]. Moreover, liposomes are the most largely used carriers within the engineered NPs approved by the Food and Drug Administration as delivery vehicles for a total of 13 compounds, including a well-known liposomal doxorubicin formulation (Doxil®) [38].

Since JQ1 is a hydrophobic molecule, it can be directly encapsulated within the lipid membrane of liposomes. Additionally, it could also be concentrated within the aqueous core by previous complexation with a β-cyclodextrin carrier. After a thorough synthetic optimisation strategy, JQ1 loading within both liposome compartments was achieved (type III JQ1-liposomes), greatly enhancing the overall loading capacity of NPs in a synergistic way and allowing reduction of sample volume and lipid amount for *in vivo* administration.

Although a preclinical investigation has reported the use of nanomaterials with selectivity towards the glomerular or tubular renal compartments [34], nanocarriers targeting the kidney for therapeutic and/or imaging purposes have not yet been clinically approved. To achieve this goal, it is crucial to modulate size and surface charge (to enable passive diffusion to kidney) and/or modify NP surfaces with targeting biomolecules such as antibodies or site-selective peptides (to enable active kidney targeting) [39-41]. The NPs described here offer potential opportunities for both therapeutics and multimodal molecular imaging (i.e., a theranostic approach) [42]. The NPs had an average size of 68 nm and negative charge at physiological pH. These physical properties should permit the NPs to reach the kidney by passive targeting and accumulate over prolonged time. Due to glomerular basement membrane pore size and negative charge properties [43] nanocarriers with size <6 nm and positive charge are expected to be

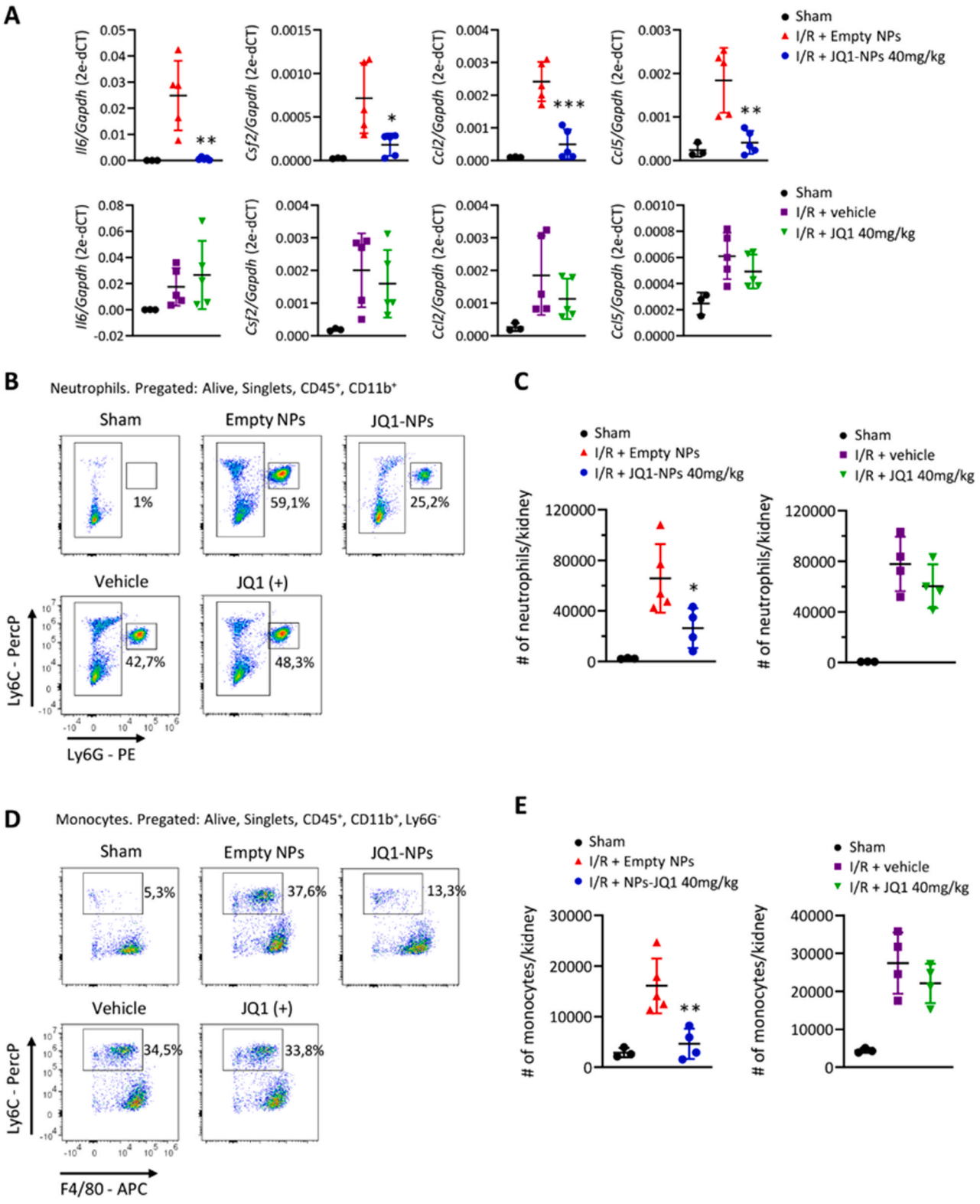

Fig. 6. Suppression of inflammation and inflammatory cell infiltration following JQ1-NP treatment. (A) Expression of proinflammatory cytokines genes were measured by qPCR in kidney samples obtained from the sham (n=3), ischemia/reperfusion (I/R) + empty nanoparticles (NPs), and the I/R + NPs-JQ1 mouse groups (n=5) at 24 h post-reperfusion. *Gapdh* was used as a control housekeeping gene. Data are summarised as the mean ± standard deviation. Statistical analyses involved use of the two-tailed Student's unpaired t-test or Mann-Whitney U test. *$p<0.05$. Representative dot plots from flow cytometry analysis of neutrophil (B) and monocyte (D) cell infiltration within the kidneys of the aforementioned mice in panel (A). Representative percentages from parents are shown. Dead cells were excluded, as well as doublets before $CD45^+$ cell gating. Complete gating strategy is shown in Supplementary Figure 6. Total cell number quantification per kidney of neutrophils (C) and monocytes (E) in the $CD45^+$-gated population was determined by TruCount Tubes. The results are means ± standard deviation of 3 (sham) to 5 (I/R) animals per group, and statistical analysis was performed using one-way ANOVA and Tukey's multiple comparisons tests. *$p<0.05$, **$p<0.01$ compared to I/R + empty NPs group. All data are representative of three experiments.

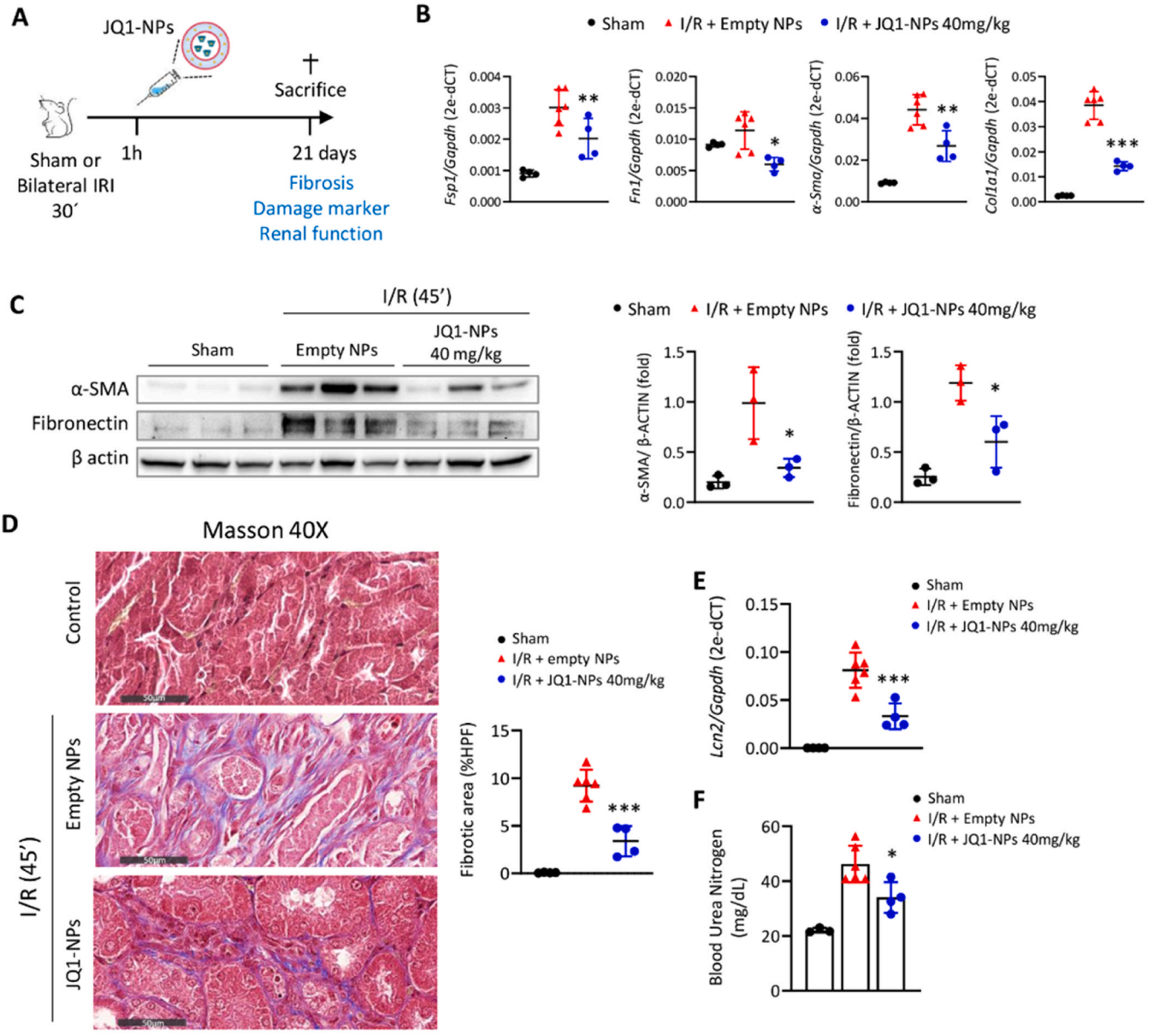

Fig. 7. Administration of JQ1-NPs following bilateral ischemia-reperfusion injury results in prevention of renal fibrosis. (A) Graphical depiction of experimental layout. 30 min ischaemic mice were administered empty nanoparticles (NPs) or JQ1-NPs at 40 mg/kg for a single boost 1 h after reperfusion and mice were sacrificed at day 21. *Gapdh* was used as a housekeeping gene. (B) Quantitative PCR analyses of fibrotic-related gene expression. (C) Western blots of α-SMA and fibronectin were performed. β-actin was used as a loading control protein. (D) Representative images of Masson's trichrome staining at day 21 in ischaemic kidneys treated as indicated with stained area quantification (%). (E) Expression level of the damage marker NGAL (*Lcn2* gene) was determined by qPCR in the kidneys and their function was estimated by the measure of blood urea nitrogen (BUN; mg/dl) serum levels (F). Values are expressed as the mean ± standard deviation of 3 (Sham) to 4–6 (I/R) animals per group. Statistical analysis was conducted with one-way ANOVA and Tukey's post-hoc tests. *$p < 0.05$, ** $p < 0.01$, *** $p < 0.001$ compared to ischemia/reperfusion (I/R) + empty NPs group. Data are representative of three independent experiments with similar findings.

cleared faster. *In vitro*, *in vivo*, and *ex vivo* characterisation indicated favourable physical properties of JQ1 liposomes and enhanced effectivity of encapsulated JQ1 in comparison to its soluble form. Additionally, considering that an ischaemic event can damage the glomerular filtration barrier whereby endothelial cells fenestrations become enlarged and microvascular permeability is altered [44], special attention was focused on determining whether the acute renal damage changed JQ1-NPs biodistribution. No significant differences in biodistribution between the sham *vs* the IRI mouse groups were observed, suggesting that type III JQ1 liposomes are potent multifunctional nanocarriers able to reach and accumulate within the kidney and promote therapeutic and imaging functions. One relevant point is that, to reach the kidney, our JQ1-NPs lack any active targeting moiety, solely relying on physical passive targeting. Hence, the surface functionalization of these NPs with specific targeting peptides is worth investigating in future studies in order to evaluate the potential enhancement of their site-selective accumulation. For example, a peptide consisting of the sequence (KKEEE)3 K which binds to the megalin receptor expressed on tubular epithelial cells has been recently described [45]. Nevertheless, we cannot undervalue the uptake of some NPs by the host mononuclear phagocytic system which reside in dedicate host filtration organs, such as the liver, spleen or lungs, being the uptake by the liver Kuppfer cells the most common mechanism through opsonization [46,47]. Toward this scope, a precise modification of NPs' surface with chemical groups able to provide stealth abilities to our nanodrugs (for example, PEG chains with different length) will be evaluated [48].

Importantly, encapsulated JQ1 showed enhanced effectivity and reduced side toxicity in comparison to its soluble form. The augmented effectiveness could be related to increased bioavailability due to kidney targeting as well as protection of JQ1 from degradation. For example, systemically administered soluble JQ1 has a half-life of only 1 h *in vivo* and therefore requires frequent dosing to promote the desired therapeutic outcome at long-term [23,49]. Reduced toxicity may be related either to reduced binding of JQ1 to plasma proteins (e.g., albumin) that ultimately undergo hepatic clearance [50] or to a reduced JQ1 peak concentration within hepatocytes due to slower drug release kinetics of liposomes. Although further experiments are required to clarify this aspect, our findings demonstrate the enhanced ability of the engineered liposomes to reduce the side toxicity of JQ1, thus overcoming one of most significant obstacles that has hampered until now the clinical translation of this promising drug in general and in the field of nephrology in particular. We are aware that, before proposing their use in humans, these JQ1-NPs should be assayed in additional models of renal damage. In this study, we selected a model of ischemia reperfusion injury, that represents one of the most physiologically relevant models as it replicates many aspects of clinical scenarios where AKI occurs, such as during kidney transplantation, cardiac surgery, or severe hypotension episodes. Exploring the efficacy of these NPs in additional models of AKI-to-CKD transition would provide valuable insights and broaden our understanding of their therapeutic potential across diverse aetiologies of kidney injury. Moreover, analysing the effect of JQ1-NPs in the models where JQ1 has already demonstrated its efficacy could shed light on whether encapsulation enables dose reduction compared to the soluble drug. Moreover, future studies need to determine the optimal therapeutic window for administering these nanoparticles and get the desired long-term effects, that may vary among the different types of kidney damage models.

One of the most relevant features of JQ1 is its anti-inflammatory characteristics which is attributed to inhibition of BRD4, a protein which activates NF-κB and expression of NF-κB-responsive pro-inflammatory genes along with neutrophil migration to the injured kidney [17,51,52]. After an IRI, tissue damage causes release of danger-associated molecular pattern (DAMP) metabolism products, which activate pattern recognition receptors that trigger sterile inflammation [53]. The production of chemokines attracts neutrophils and monocytes that are responsible for microvasculature congestion, impaired renal blood flow and prolonged ischaemic injury [54,55]. The initial immune cell infiltration is triggered very quickly after injury, thus, blocking this initial step in the inflammatory cascade is expected to enable therapeutic benefits as previously described [56,57] and supported in this work.

Our results showed that a single dose of JQ1-NPs not only improved kidney function but also halted progression of CKD. This could be due to two possible scenarios: an inflammatory cascade reduction and/or inhibition of maladaptive mechanisms within the kidney. The immune response is necessary for tissue repair, but if it persists too long time or the damage is severe, it can speed up the development and progression of CKD [58]. Thus, reduction of the inflammatory response within the kidney stroma observed in JQ1-NPs-treated mice after IRI could explain inhibition of CKD progression. For the second scenario, the maladaptive repair mechanisms that drive CKD progression after ischaemic AKI include cell cycle arrest of tubular epithelial cells, which secrete pro-fibrotic factors and become senescent [6] and loss of capillary density generates chronic hypoxia and hypertension. These events further worsen the initial damage and promote disease progression and organ malfunction [7]. In this context, future studies employing single-cell technology will be of great interest to understand the precise mechanisms of JQ1 action within specific cell types and to explore the detailed interactions of JQ1 at the cellular level. JQ1-mediated down-regulation of BRD4 has antifibrotic effects due to inhibition of both TGFβ-induced signalling pathways and epithelial-to-mesenchymal transition-related protein expression [15,18-20]. Moreover, JQ1 has been shown to suppress: i) the DNA damage response and oxidative/-nitrosative stress pathways in tubular epithelial cells [22]; ii) through its activity as c-myc inhibitor, the metabolic switch that kidney stromal cells require for the development of progressive tubulointerstitial fibrosis downstream of IL-1β signalling [59]; and iii) IRI-induced tubular cell apoptosis and endoplasmic reticulum stress activation [21]. While these studies have analysed the role of BRD4 in AKI or CKD as independent physio-pathological processes, our work demonstrates the JQ1-mediated inhibition of AKI as a necessary previous step to block CKD transition in bilateral renal IRI.

Encapsulation within engineered liposomes may represent a solution to exploit the therapeutic potential of BET inhibitors. However, before translational application in nephrology can occur, several challenges must be overcome such as improvement in *in vivo* stability, enhancement of kidney targeting and biodistribution, and determine the correct time of administration [60]. Addressing these challenges will require continued research and development in the field of nanoparticle-based renal drug delivery.

5. Conclusions

To our knowledge, this study represents the first exploration of JQ1-loaded liposomes in the context of nephrology. With a dedicated focus on enhancing therapeutic outcomes, we optimized the synthesis of these liposomes to bolster JQ1's stability and bioavailability within the kidney. Our innovative nanoformulation approach facilitated higher loading capacity and enabled both membrane and core encapsulation, leading to a synergistic yield of encapsulated JQ1. Our findings underscore the enhanced effectiveness of encapsulated JQ1 when compared to its soluble form, assessed in the mouse AKI model of ischemia-reperfusion injury. Importantly, with only one administration of our JQ1-loaded nanoparticles, we effectively decreased the immune cell infiltration in the kidney—an early and pivotal step to prevent damage progression. This success not only improved immediate kidney function but, most remarkably, halted fibrosis development and the progression to CKD. Thus, this research represents a significant step forward in the development of an innovative therapy for AKI and CKD. Our pioneering liposomal formulation not only expands the therapeutic potential of JQ1 but also addresses a significant barrier to its clinical translation in the nephrology field.

Funding

This study has been funded by Instituto de Salud Carlos III (ISCIII) through the projects No DTS20/00109 (AES20-ISCIII), PI19/00184, PI20/00639, PI22/00738 and PI22/00789 co-funded by the European Union; Adquisición de equipamiento e Infraestructuras científico-técnicas (IFEQ21/00203) and RICORS program to RICORS2040 (Kidney Disease, RD21/0005/0017) funded by European Union with charge to NextGenerationEU that finance the actions of the Mechanism for Recovery and Resilience (MRR)/RETC; PCTI-Plan de Ciencia, Tecnología e Innovación 2021–2023 del Gobierno del Principado de Asturias/FEDER (Grant number IDI/2021/000032); Sociedad Española de Nefrología SEN 2022, Ayudas a la Investigación en Nefrología, Proyecto "NANO-BET" to B S-A. L.L-C., M.F. and M.M. acknowledge the support of Microscopy & Dynamic Imaging Unit of CNIC, Madrid, Spain. The Unit is part of the ReDiB-ICTS and has the support of FEDER, "Una manera de hacer Europa." The CNIC is supported by the Instituto de Salud Carlos III (ISCIII), the Ministerio de Ciencia e Innovación (MCIN) and the Pro CNIC Foundation, and is a Severo Ochoa Center of Excellence (grant CEX2020–001041-S funded by MICIN/AEI/10.13039/501100011033). Sara Borrell' program (grant number CD20/00042 to R.R.R.-D.) and Miguel Servet Iprogram (grant number CP18/00106 to B.S.-A.) from ISCIII. A.B.F (BP20–143) and C.R-B (BP21/044) received a Severo Ochoa Grant from Programa de Ayudas "Severo Ochoa" para la formación en investigación y docencia del Principado de Asturias,

Gobierno del Principado de Asturias. P.D.-B. has been supported by Red de Investigación Renal REDINRED, grant number RD21/0005/0017, ISCIII; M.L.S. by FEDER-PCTI 2021–2023, Gobierno del Principado de Asturias (grant number IDI/2021/000032) and R.M.R was supported by a postdoctoral grant from the Scientific Foundation of the Spanish Association Against Cancer (INVES222995RODR). L.L.-C., M.M. and M.F. would like to thank Comunidad de Madrid for the predoctoral grant IND2020/BIO-17523 of L.L.-C.

CRediT authorship contribution statement

Raul R Rodrigues-Diez: Methodology, Investigation. **Cristian Ruiz Bernet:** Methodology, Investigation. **Mar Rodriguez-Santamaria:** Methodology, Investigation. **Cristina Martin-Martin:** Methodology, Investigation. **Ramon M. Rodriguez:** Methodology, Investigation. **Maria Laura Saiz:** Writing – review & editing, Writing – original draft, Methodology, Investigation, Formal analysis, Data curation. **Ivan Fernandez-Vega:** Methodology, Investigation. **Beatriz Suarez-Alvarez:** Writing – review & editing, Writing – original draft, Validation, Supervision, Methodology, Investigation, Formal analysis, Data curation, Conceptualization. **Aida Bernardo Florez:** Methodology, Investigation. **Carmen Diaz-Corte:** Methodology, Investigation. **Laura Lozano-Chamizo:** Writing – review & editing, Writing – original draft, Methodology, Investigation, Formal analysis, Data curation. **Carlos Lopez-Larrea:** Writing – review & editing, Writing – original draft, Validation, Supervision, Resources, Funding acquisition, Formal analysis, Data curation, Conceptualization. **Paula Diaz-Bulnes:** Methodology, Investigation. **Marco Filice:** Writing – review & editing, Writing – original draft, Validation, Supervision, Resources, Project administration, Funding acquisition, Formal analysis, Data curation, Conceptualization. **Marzia Marciello:** Writing – original draft, Methodology, Investigation. **Viviana Corte-Iglesias:** Methodology, Investigation.

Declaration of Competing Interest

The authors declare that they have no known competing financial interests or personal relationships that could have appeared to influence the work reported in this paper.

Data availability

Data will be made available on request.

Acknowledgements

The authors acknowledge the editorial assistance, in the form of language editing and correction, provided by XpertScientific Editing and Consulting Services.

Available of data

The main data supporting the results of this study are available within the papers and its Supplementary Information. The raw and analysed datasets generated during the study are available for research purposes from the corresponding authors on reasonable request.

Appendix A. Supporting information

Supplementary data associated with this article can be found in the online version at doi:10.1016/j.biopha.2024.116492.

References

[1] N.H. Lameire, A. Levin, J.A. Kellum, M. Cheung, M. Jadoul, W.C. Winkelmayer, et al., Harmonizing acute and chronic kidney disease definition and classification: report of a Kidney Disease: improving global outcomes (KDIGO) consensus conference, Kidney Int 100 (3) (2021 Sep) 516–526.
[2] F. Turgut, A.S. Awad, E.M. Abdel-Rahman, Acute kidney injury: medical causes and pathogenesis, J. Clin. Med 12 (1) (2023 Jan 3).
[3] G.M. Chertow, E. Burdick, M. Honour, J. v Bonventre, D.W. Bates, Acute kidney injury, mortality, length of stay, and costs in hospitalized patients, J. Am. Soc. Nephrol. 16 (11) (2005 Nov) 3365–3370.
[4] L.S. Chawla, P.W. Eggers, R.A. Star, P.L. Kimmel, Acute kidney injury and chronic kidney disease as interconnected syndromes, N. Engl. J. Med 371 (1) (2014 Jul) 58–66.
[5] E.J. See, K. Jayasinghe, N. Glassford, M. Bailey, D.W. Johnson, K.R. Polkinghorne, et al., Long-term risk of adverse outcomes after acute kidney injury: a systematic review and meta-analysis of cohort studies using consensus definitions of exposure, Kidney Int 95 (1) (2019 Jul) 160–172.
[6] D.A. Ferenbach, J.V. Bonventre, Mechanisms of maladaptive repair after AKI leading to accelerated kidney ageing and CKD, Nat. Rev. Nephrol. 11 (5) (2015 May) 264–276.
[7] Z. Wang, C. Zhang, From AKI to CKD: Maladaptive repair and the underlying mechanisms, Int J. Mol. Sci. 23 (18) (2022 Sep 17).
[8] C. Guo, G. Dong, X. Liang, Z. Dong, Epigenetic regulation in AKI and kidney repair: mechanisms and therapeutic implications, Nat. Rev. Nephrol. 15 (4) (2019 Apr) 220–239.
[9] P. Filippakopoulos, S. Picaud, M. Mangos, T. Keates, J.P. Lambert, D. Barsyte-Lovejoy, et al., Histone recognition and large-scale structural analysis of the human bromodomain family, Cell 149 (1) (2012 Mar 30) 214–231.
[10] O. Bechter, P. Schöffski, Make your best BET: the emerging role of BET inhibitor treatment in malignant tumors, Pharm. Ther. 208 (2020 Apr) 107479.
[11] Q. Duan, S. McMahon, P. Anand, H. Shah, S. Thomas, H.T. Salunga, et al., BET bromodomain inhibition suppresses innate inflammatory and profibrotic transcriptional networks in heart failure, Sci. Transl. Med 9 (390) (2017 May 17).
[12] Q. gang Zhang, J. Qian, Y. chang Zhu, Targeting bromodomain-containing protein 4 (BRD4) benefits rheumatoid arthritis, Immunol. Lett. 166 (2) (2015 Aug) 103–108.
[13] Y. Li, J. Xiang, J. Zhang, J. Lin, Y. Wu, X. Wang, Inhibition of Brd4 by JQ1 promotes functional recovery from spinal cord injury by activating autophagy, Front Cell Neurosci. 14 (2020) 555591.
[14] L. Tejedor-Santamaria, J.L. Morgado-Pascual, L. Marquez-Exposito, B. Suarez-Alvarez, R.R. Rodrigues-Diez, A. Tejera-Muñoz, et al., Epigenetic Modulation of Gremlin-1/NOTCH pathway in experimental crescentic immune-mediated glomerulonephritis, Pharmaceuticals 15 (2) (2022 Jan 20).
[15] J.L. Morgado-Pascual, B. Suarez-Alvarez, V. Marchant, P. Basantes, P.L. Tharaux, A. Ortiz, et al., Type IV Collagen and SOX9 are molecular targets of BET inhibition in experimental glomerulosclerosis, Int. J. Mol. Sci. 24 (1) (2022 Dec 28).
[16] H. Zuo, S. Wang, J. Feng, X. Liu, BRD4 contributes to high-glucose-induced podocyte injury by modulating Keap1/Nrf2/ARE signaling, Biochimie 165 (2019 Oct) 100–107.
[17] B. Suarez-Alvarez, J.L. Morgado-Pascual, S. Rayego-Mateos, R.M. Rodriguez, R. Rodrigues-Diez, P. Cannata-Ortiz, et al., Inhibition of bromodomain and extraterminal domain family proteins ameliorates experimental renal damage, J. Am. Soc. Nephrol. 28 (2) (2017 Feb) 504–519.
[18] S. Tao, S. Tao, F. Guo, L. Zhang, L. Zhao, P. Fu, et al., Discovery of indol-6-yl-pyrrolo[2,3-c]pyridin-7-one derivatives as bromodomain-containing protein 4 (BRD4) inhibitors for the treatment of kidney fibrosis, Eur. J. Med Chem. 231 (2022 Mar 5) 114153.
[19] X. Wang, Y. Zhou, Y. Peng, T. Huang, F. Xia, T. Yang, et al., Bromodomain-containing protein 4 contributes to renal fibrosis through the induction of epithelial-mesenchymal transition, Exp. Cell Res. 383 (2) (2019 Oct 15) 111507.
[20] B. Zhou, J. Mu, Y. Gong, C. Lu, Y. Zhao, T. He, et al., Brd4 inhibition attenuates unilateral ureteral obstruction-induced fibrosis by blocking TGF-β-mediated Nox4 expression, Redox Biol. 11 (2017 Apr) 390–402.
[21] H. Liu, L. Wang, X. Weng, H. Chen, Y. Du, C. Diao, et al., Inhibition of Brd4 alleviates renal ischemia/reperfusion injury-induced apoptosis and endoplasmic reticulum stress by blocking FoxO4-mediated oxidative stress, Redox Biol. 24 (2019 Jun) 101195.
[22] L. Sun, J. Liu, Y. Yuan, X. Zhang, Z. Dong, Protective effect of the BET protein inhibitor JQ1 in cisplatin-induced nephrotoxicity, Am. J. Physiol. Ren. Physiol. 315 (3) (2018 Sep 1) F469–F478.
[23] P. Filippakopoulos, J. Qi, S. Picaud, Y. Shen, W.B. Smith, O. Fedorov, et al., Selective inhibition of BET bromodomains, Nature 468 (7327) (2010 Dec 24) 1067–1073.
[24] H. Wang, W. Huang, M. Liang, Y. Shi, C. Zhang, Q. Li, et al., +)-JQ1 attenuated LPS-induced microglial inflammation via MAPK/NFκB signaling, Cell Biosci. 8 (1) (2018 Dec 20) 60.
[25] T. Shorstova, W.D. Foulkes, M. Witcher, Achieving clinical success with BET inhibitors as anti-cancer agents, Br. J. Cancer 124 (9) (2021 Apr 27) 1478–1490.
[26] D.A. Mele, A. Salmeron, S. Ghosh, H.R. Huang, B.M. Bryant, J.M. Lora, BET bromodomain inhibition suppresses TH17-mediated pathology, J. Exp. Med. 210 (11) (2013 Oct 21) 2181–2190.
[27] E. Kulikowski, B.D. Rakai, N.C.W. Wong, Inhibitors of bromodomain and extra-terminal proteins for treating multiple human diseases, Med Res Rev. 41 (1) (2021 Jan 14) 223–245.
[28] A.G. Cochran, A.R. Conery, R.J. Sims, Bromodomains: a new target class for drug development, Nat. Rev. Drug Discov. 18 (8) (2019 Aug) 609–628.
[29] K. Ovejero-Paredes, D. Díaz-García, I. Mena-Palomo, M. Marciello, L. Lozano-Chamizo, Y.L. Morato, S. Prashar, S. Gómez-Ruiz, M. Filice, Synthesis of a theranostic platform based on fibrous silica nanoparticles for the enhanced treatment of triple-negative breast cancer promoted by a combination of chemotherapeutic agents, Biomater. Adv. 137 (2022 Jun) 212823.

[30] A. Linkermann, J.H. Bräsen, M. Darding, M.K. Jin, A.B. Sanz, J.O. Heller, et al., Two independent pathways of regulated necrosis mediate ischemia-reperfusion injury, Proc. Natl. Acad. Sci. USA 110 (29) (2013 Jul 16) 12024–12029.
[31] J.K. Patra, G. Das, L.F. Fraceto, E.V.R. Campos, M. del P. Rodriguez-Torres, L. S. Acosta-Torres, et al., Nano based drug delivery systems: recent developments and future prospects, J. Nanobiotechnology 16 (1) (2018 Dec 19) 71.
[32] S. Hejmady, R. Pradhan, A. Alexander, M. Agrawal, G. Singhvi, B. Gorain, et al., Recent advances in targeted nanomedicine as promising antitumor therapeutics, Drug Discov. Today 25 (12) (2020 Dec) 2227–2244.
[33] M.J. Mitchell, M.M. Billingsley, R.M. Haley, M.E. Wechsler, N.A. Peppas, R. Langer, Engineering precision nanoparticles for drug delivery, Nat. Rev. Drug Discov. 20 (2) (2021 Feb) 101–124.
[34] P. Paluszkiewicz, A. Martuszewski, N. Zaręba, K. Wala, M. Banasik, M. Kepinska, The application of nanoparticles in diagnosis and treatment of kidney diseases, Int J. Mol. Sci. 23 (1) (2021 Jul).
[35] V. Maggisano, M. Celano, R. Malivindi, I. Barone, D. Cosco, C. Mio, et al., Nanoparticles loaded with the BET Inhibitor JQ1 Block the Growth of Triple Negative Breast Cancer Cells In Vitro and In Vivo, Cancers (Basel) 12 (1) (2019 Dec 30) 91.
[36] F.C. Lam, S.W. Morton, J. Wyckoff, T.L.V. Han, M.K. Hwang, A. Maffa, et al., Enhanced efficacy of combined temozolomide and bromodomain inhibitor therapy for gliomas using targeted nanoparticles, Nat. Commun. 9 (1) (2018 Jul) 1991.
[37] T. Wang, H. Zhang, Y. Han, Q. Zheng, H. Liu, M. Han, et al., Reversing T cell dysfunction to boost glioblastoma immunotherapy by paroxetine-mediated GRK2 inhibition and blockade of multiple checkpoints through biomimetic nanoparticles, Adv. Sci. (Weinh.) 10 (9) (2023 Jul) e2204961.
[38] Y. Barenholz, Doxil®–the first FDA-approved nano-drug: lessons learned, J. Control Release 160 (2) (2012 Jul) 117–134.
[39] Y. Huang, K. Jiang, X. Zhang, E.J. Chung, The effect of size, charge, and peptide ligand length on kidney targeting by small, organic nanoparticles, Bioeng. Transl. Med. 5 (3) (2020 Sep) e10173.
[40] Y. Huang, J. Wang, K. Jiang, E.J. Chung, Improving kidney targeting: The influence of nanoparticle physicochemical properties on kidney interactions, J. Control Release 334 (2021 Jun 10) 127–137.
[41] J. Wang, J.J. Masehi-Lano, E.J. Chung, Peptide and antibody ligands for renal targeting: nanomedicine strategies for kidney disease, Biomater. Sci. 5 (8) (2017 Jul 25) 1450–1459.
[42] M. Marciello, J. Pellico, I. Fernandez-Barahona, F. Herranz, J. Ruiz-Cabello, M. Filice, Recent advances in the preparation and application of multifunctional iron oxide and liposome-based nanosystems for multimodal diagnosis and therapy, Interface Focus 6 (6) (2016 Dec) 20160055, 6.
[43] B. Du, M. Yu, J. Zheng, Transport and interactions of nanoparticles in the kidneys, Nat. Rev. Mater. 3 (10) (2018 Aug) 358–374, 3.
[44] T.A. Sutton, Alteration of microvascular permeability in acute kidney injury, Micro Res. 77 (1) (2009 Jan) 4–7.
[45] A. Wischnjow, D. Sarko, M. Janzer, C. Kaufman, B. Beijer, S. Brings, et al., Renal targeting: peptide-based drug delivery to proximal tubule cells, Bioconj Chem. 27 (4) (2016 Apr 20) 1050–1057.
[46] H.H. Holt-Casper, D. Grainger, D.W. Ghandehari H, Nanoparticle uptake: the phagocyte problem, Nano Today 10 (4) (2015 Aug) 487–510.
[47] S.M. Moghimi SM, J. Stealth, liposomes and long circulating nanoparticles: critical issues in pharmacokinetics, opsonization and protein-binding properties, Prog. Lipid Res 42 (6) (2023 Nov) 463–478.
[48] A. Lazaro-Carrillo, M. Filice, M.J. Guillén, R. Amaro, M. Viñambres, A. Tabero, K. O. Paredes, A. Villanueva, P. Calvo, M. Del Puerto Morales, M. Marciello, Tailor-made PEG coated iron oxide nanoparticles as contrast agents for long lasting magnetic resonance molecular imaging of solid cancers, Mater. Sci. Eng. C. Mater. Biol. Appl. 107 (2020 Feb) 110262.
[49] M.M. Matzuk, M.R. McKeown, P. Filippakopoulos, Q. Li, L. Ma, J.E. Agno, et al., Small-molecule inhibition of BRDT for male contraception, Cell 150 (4) (2012 Aug 17) 673–684.
[50] M. Boffito, D.J. Back, C. Flexner, P. Sjö, T.F. Blaschke, P.W. Horby, et al., Toward consensus on correct interpretation of protein binding in plasma and other biological matrices for COVID-19 therapeutic development, Clin. Pharm. Ther. 110 (1) (2021 Jul) 64–68.
[51] S. Reid, N. Fine, V.K. Bhosle, J. Zhou, R. John, M. Glogauer, et al., Inhibition of BRD4 reduces neutrophil activation and adhesion to the vascular endothelium following ischemia reperfusion injury, Int J. Mol. Sci. 21 (24) (2020 Dec 17).
[52] B. Huang, X.D. Yang, M.M. Zhou, K. Ozato, L.F. Chen, Brd4 coactivates transcriptional activation of NF-kappaB via specific binding to acetylated RelA, Mol. Cell Biol. 29 (5) (2009 Mar) 1375–1387.
[53] H. Kono, K.L. Rock, How dying cells alert the immune system to danger, Nat. Rev. Immunol. 8 (4) (2008 Apr) 279–289.
[54] J.V. Bonventre, L. Yang, Cellular pathophysiology of ischemic acute kidney injury, J. Clin. Invest 121 (11) (2011 Nov) 4210–4221.
[55] T.M. Williams, A.F. Wise, D.S. Layton, S.D. Ricardo, Phenotype and influx kinetics of leukocytes and inflammatory cytokine production in kidney ischemia/reperfusion injury, Nephrol. (Carlton) 23 (1) (2018 Jan) 75–85.
[56] L. Li, L. Huang, S.S.J. Sung, A.L. Vergis, D.L. Rosin, C.E. Rose, et al., The chemokine receptors CCR2 and CX3CR1 mediate monocyte/macrophage trafficking in kidney ischemia-reperfusion injury, Kidney Int 74 (12) (2008 Dec) 1526–1537.
[57] S. Chaturvedi, D.A. Yuen, A. Bajwa, Y.W. Huang, C. Sokollik, L. Huang, et al., Slit2 prevents neutrophil recruitment and renal ischemia-reperfusion injury, J. Am. Soc. Nephrol. 24 (8) (2013 Jul) 1274–1287.
[58] Y. Sato, M. Yanagita, Immune cells and inflammation in AKI to CKD progression, Am. J. Physiol. Ren. Physiol. 315 (6) (2018 Dec 1) F1501–F1512.
[59] D.R. Lemos, M. McMurdo, G. Karaca, J. Wilflingseder, I.A. Leaf, N. Gupta, et al., Interleukin-1β Activates a MYC-dependent metabolic switch in kidney stromal cells necessary for progressive tubulointerstitial fibrosis, J. Am. Soc. Nephrol. 29 (6) (2018 Jun) 1690–1705.
[60] J.P.J. Merlin, X. Li, Role of nanotechnology and their perspectives in the treatment of kidney diseases, Front Genet 12 (2022 Jan 5).